Optimizing the use of a sensor resource for opponent polarization coding

Francisco J. H. Heras[1] **and Simon B. Laughlin**[1]

[1]Department of Zoology, University of Cambridge, Cambridge CB2 3EJ, UK

ABSTRACT

Flies use specialized photoreceptors R7 and R8 in the dorsal rim area (DRA) to detect skylight polarization. R7 and R8 form a tiered waveguide (rhabdom) with R7 on top, filtering light delivered to R8. We examine how the division of a given resource, rhabdom length, between R7 and R8 affects their ability to code polarization angle. We model optical absorption to show how the length fractions allotted to R7 and R8 determine the rates at which they transduce photons, and correct these rates for transduction unit saturation. The rates give polarization signal and photon noise in R7, and in R8. Their signals are combined in an opponent unit, intrinsic noise added, and the unit's output analysed to extract two measures of coding ability, number of discriminable polarization angles and mutual information. A very long R7 maximizes opponent signal amplitude, but codes inefficiently due to photon noise in the very short R8. Discriminability and mutual information are optimized by maximizing signal to noise ratio, SNR. At lower light levels approximately equal lengths of R7 and R8 are optimal because photon noise dominates. At higher light levels intrinsic noise comes to dominate and a shorter R8 is optimum. The optimum R8 length fractions falls to one third. This intensity dependent range of optimal length fractions corresponds to the range observed in different fly species and is not affected by transduction unit saturation. We conclude that a limited resource, rhabdom length, can be divided between two polarization sensors, R7 and R8, to optimize opponent coding. We also find that coding ability increases sub-linearly with total rhabdom length, according to the law of diminishing returns. Consequently the specialized shorter central rhabdom in the DRA codes polarization twice as efficiently with respect to rhabdom length than the longer rhabdom used in the rest of the eye.

Keywords: fly, dorsal rim, photoreceptor length, photon noise, discriminable polarization angles, jnd

INTRODUCTION

Sunlight is polarized by scattering and reflection, and many animals take advantage of this to guide tasks such as orientation, prey detection and water surface detection (Wehner, 2001). To detect polarization patterns in the sky, many insects use a specialised region in the eye, the Dorsal Rim Area (DRA) (Labhart and Meyer, 1999). In flies, the DRA is a narrow band of ommatidia along the dorsal margin of the eye, containing specialised central photoreceptors R7 and R8 (Wada, 1974a). The microvilli of rhabdomeric photoreceptors are intrinsically dichroic (Moody and Parriss, 1961; Snyder and Laughlin, 1975), but elsewhere in the eye the polarization sensitivity (PS) of the photoreceptors is suppressed by rhabdomere twist (Smola and Tscharntke, 1979). In the DRA, however, the rhabdomeres of R7 and R8 are not twisted (Wunderer and Smola, 1982a), and thus they present high PS (Hardie, 1984).

In the DRA, R7 and R8 form a pair of orthogonal polarization analysers with identical UV sensitivities, sampling the same small area of the sky (Hardie, 1985). The axons of both R7 and R8 in the same DRA ommatidium project retinotopically to a specific region within the medulla (Strausfeld and Wunderer, 1985; Fortini and Rubin, 1991), where their signals are compared to extract information about polarization. This comparison most likely involves polarization-opponent neurons, as found in some species of ants, locusts and crickets (Labhart, 1988, 2000; Labhart et al., 2001; Vitzthum et al., 2002).

Several conflicting parameters determine the quality of the photoreceptor signal. In most flies, the photosensitive membranes —rhabdomeres— of R7 and R8 form a tiered waveguide, the central rhabdom (Figure 1). The pair of rhabdomeres lie at the center of the ommatidium, and in axial section they are surrounded by the R1-6 achromatic rhabdomeres that form a waveguide each. The rhabdomere of R7 sits on top of the rhabdomere of R8, and thereby filters the light available to R8. A longer R7 rhabdomere
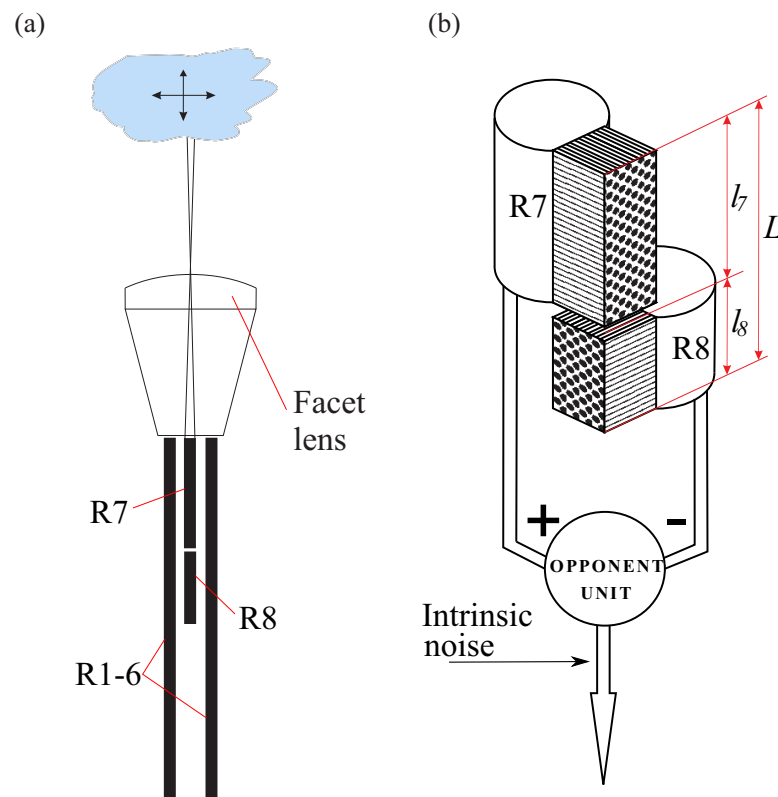
Figure 1. Optical sampling and opponent coding by R7 and R8 in fly DRA. (a) Diagramatic longitudinal section of an ommatidium in DRA showing R7/R8's central rhabdom, with two of six outer photoreceptors, type R1-6. Note central rhabdom is much shorter in DRA. R7 and R8 sample same small area of the sky, focused onto R7 by facet lens, and R7 filters light received R8. (b) Opponent coding. R8's microvilli are perpendicular to R7's, giving orthogonal polarization sensitivities and enhancement of R8's signal by absorption in R7. Opponent unit outputs difference between inpts from R7 and R8, and adds intrinsic noise.

47 increases the PS of R8 (Snyder, 1973; Gribakin and Govardovskii, 1975; Menzel, 1975; Hardie, 1984)
48 but reduces its own PS by self-screening (Snyder, 1973; Nilsson et al., 1987). The quality of the signal
49 coded by a photoreceptor is also limited by the quantum nature of the light. A longer rhabdomere will be
50 less affected by photon noise than a shorter one because it absorbs more photons (Warrant and Nilsson,
51 1998), and has more transduction units (microvilli) to convert photons into electrical signals (Howard
52 et al., 1987; Anderson and Laughlin, 2000). However, because the rhabdomeres of R7 and R8 share the
53 length of a central rhabdom of given length, it is not possible to increase the length of both photoreceptors
54 simultaneously, lengthening one shortens the other.

55 To investigate how these length dependent trade-offs between polarization sensitivity and photon noise
56 influence the ability of the fly DRA to code polarization, we used a modelling procedure adapted from
57 color vision (Vorobyev et al., 1998; Osorio and Vorobyev, 1996) and recently applied to polarization vision
58 (How and Marshall, 2014). We find that for a central rhabdom of fixed length, polarization sensitivity and
59 signal coded by a polarization-opponent unit are highest when R8 is as short as possible. On the other
60 hand, measures of discrimination that consider signal and two forms of noise, photon and intrinsic, are
61 highest for intermediate values of R7 and R8 lengths, broadly agreeing with the experimental evidence
62 (Wada, 1974a; Wunderer and Smola, 1982a). We conclude that it is essential to consider photon and
63 intrinsic noise when analyzing the ability of tiered photoreceptors to support behaviour. When this is done
64 we see that the distribution of a sensor resource, photoreceptor length, can be optimized for opponent
65 coding.

METHODS
66

Photon absorption rates and polarization sensitivity
67

68 An optical model gives the rates at which R7 and R8 absorb photons when sampling a small patch of blue
69 sky.

Photons available from skylight
70

71 To sample a small patch of sky, the facet lens focuses skylight onto the entrance aperture of R7 (Figure 1).
72 The spectral flux of photons at R7's entrance aperture is (e.g. Johnsen 2012, Chapter 4)

$$N_i(\lambda) = \left(\frac{\pi}{4}\right)^2 \left(\frac{1}{F}\right)^2 D_r^2 L(\lambda) \tag{1}$$

73 where F, the facet lens's F-ratio, is the focal length of the facet lens divided by its diameter, D_r is the
74 rhabdomere diameter and $L(\lambda)$ is the spectral radiance of skylight.

75 The spectral radiance of the sky is equivalent to the radiance of an ideal diffusely reflecting (Lamber-
76 tian) surface illuminated by cloudless sky, with the sun occluded (Johnsen, 2012, Chapter 9). To obtain
77 spectral radiance we converted suitable measurements of spectral irradiance ($\mathrm{W\,m^{-2}\,nm^{-1}}$) —taken at
78 noon on a cloudless summer's day in Pretoria, South Africa (Kok, 1972)— to spectral radiance $L(\lambda)$,
79 (photons $\mathrm{sr^{-1}\,m^{-2}\,nm^{-1}}$) by dividing by π and the quantal energy $h\nu = hc/\lambda$.

80 R7 and R8 capture photons with a UV rhodopsin that absorbs significantly between 300 nm and
81 412 nm (Figure 2). Consequently the flux of available photons at R7's entrance aperture is

$$N_i = \int_{300\,\mathrm{nm}}^{412\,\mathrm{nm}} \left(\frac{\pi}{4}\right)^2 \left(\frac{1}{F}\right)^2 D_r^2 L(\lambda) d\lambda \tag{2}$$

82 Given measured values, $F = 2$, $D_r = 1.9\,\mu\mathrm{m}$ and the spectral radiance for skylight (as obtained above),
83 N_i is 1.6×10^7 photons $\mathrm{s^{-1}}$ on a bright summer's day.

Photon absorption rates
84

85 R7's photon absorption rate, N_7, depends upon N_i, the photon flux incident onto R7's entrance aperture,
86 the absorption coefficients of R7's rhabdomere and its length. To account for polarization we decompose
87 the light entering R7 into a pair of orthogonal e-vectors, one parallel and the other perpendicular to R7's
88 microvilli. Given an incident flux of N_i photons $\mathrm{s^{-1}}$, partially polarized, with degree d and angle θ,
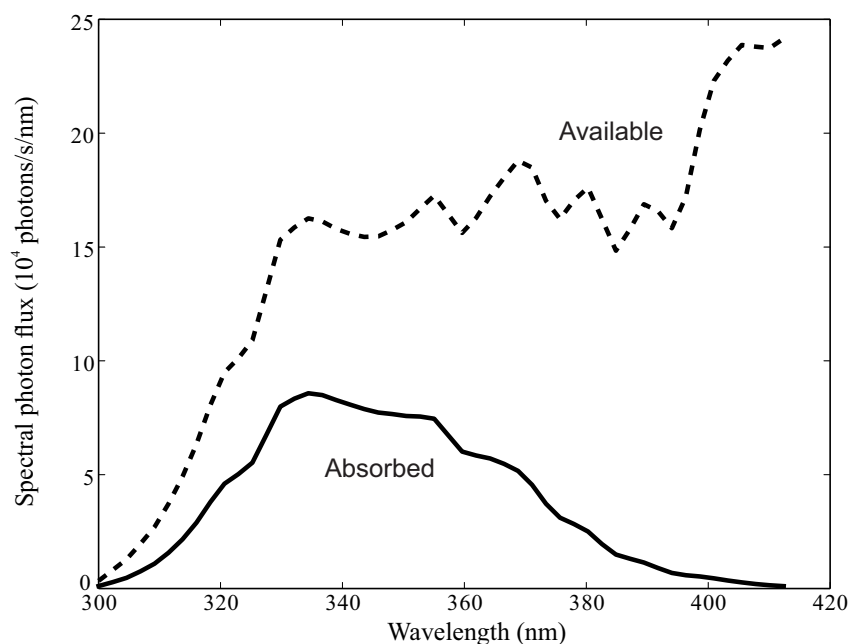
Figure 2. Spectral photon flux delivered by facet lens to tip of R7 rhabdomere (dashed line), and photons absorbed by rhodopsin molecules in R7 and R8 (solid line). Lens views cloudless blue sky in summer, in Pretoria (Kok, 1972). Lens F-ratio = 2; rhabdomere diameter 1.9 μm; rhabdom length (length of R7 plus R8) $L = 100$ μm; absorption by rhodopsin with single peak at wavelength 335 nm; absorption coefficient of rhabdom at peak wavelength $k = 0.0075$ μm^{-1}.

$$N_\parallel = N_i \frac{1 + d\cos(2\theta)}{2} \tag{3}$$

and

$$N_\perp = N_i \frac{1 - d\cos(2\theta)}{2} \tag{4}$$

It follows that for light of wavelength λ

$$N_7(\lambda) = (1 - e^{-k_\parallel(\lambda)l_7})N_\parallel(\lambda) + (1 - e^{-k_\perp(\lambda)l_7})N_\perp(\lambda) \tag{5}$$

where $k_\parallel(\lambda)$ is the absorption coefficient for light polarized parallel the microvilli, $k_\perp(\lambda)$ is for light polarized perpendicularly, and l_7 is the length of R7's rhabdomere.

R8 receives the light that passes through R7 with microvilli that are perpendicular to R7's. Consequently, R8's photon absorption rate is given by (Snyder, 1973):

$$N_8(\lambda) = e^{-k_\parallel(\lambda)l_7}(1 - e^{-k_\perp(\lambda)l_8})N_\parallel(\lambda) + e^{-k_\perp(\lambda)l_7}(1 - e^{-k_\parallel(\lambda)l_8})N_\perp(\lambda) \tag{6}$$

We assume that the rhabdomeres of R7 and R8 have the same absorption coefficient $k_\parallel(\lambda)$ and $k_\perp(\lambda)$, and a dichroic ratio

$$\delta = k_\parallel(\lambda)/k_\perp(\lambda) \tag{7}$$

that is independent of wavelength. Both absorption coefficients peak at a wavelength, $\lambda_{max} = 335\,\text{nm}$ (Hardie and Kirschfeld, 1983; Hardie, 1985).

Non-monochromatic light absorption

Skylight is not monochromatic. In that case, absorption by R7 and R8 is obtained by integrating equations 5 and 6 with respect to wavelength (Johnsen, 2012, Chapter 4). Whereas the absorption of monochromatic light is an exponential function of rhabdomere length, l (equations 5 and 6) total absorption is not. The absorptance, the fraction of absorbed photons increases with rhabomere length, l, according to a function whose form is uniquely dependent upon the rhabdomere absorption spectrum and the spectrum of incoming light.

$$F_a(\kappa) = \frac{1}{N_i} \int (1 - e^{-k(\lambda)l})N_i(\lambda)d\lambda \tag{8}$$

To simplify our calculations we followed Warrant and Nilsson (1998) and approximated this unique function. The fraction of photons absorbed by a photoreceptor of length l and maximum absorption coefficient $k(\lambda_{max})$ increases with the product of $k(\lambda_{max})$ and l, $\kappa = k(\lambda_{max})l$ according to function, $F_a(\kappa)$.

We approximated $F_a(\kappa)$ as follows. Using the absorption template of rhodopsin (Stavenga et al., 1993) with a single peak absorption at 335 nm (Hardie and Kirschfeld, 1983), and $L(\lambda)$, the spectral radiance of blue skylight, we calculated the fraction of absorbed photons for a number of values of κ. We then fitted a function to these points,

$$F_a(\kappa) = (1 - e^{-\kappa})\left[0.4697838 + 0.05512361\kappa - 0.00291346\kappa^2\right] \tag{9}$$

which approximated the true length dependency with relative error $< 1\%$, for photoreceptor lengths up to 1 mm (Figure 3).

In comparison, adapting Warrant and Nilsson (1998) approximation by extrapolating its coefficients would produce a reasonable approximation for medium length photoreceptors (Figure 3) but would not have produced the right behaviour in the limit of very short photoreceptors. Consequently, the PS of very short photoreceptors calculated with Warrant and Nilsson (1998) approximation would not be its intrinsic PS, i.e. its dichroic ratio δ.
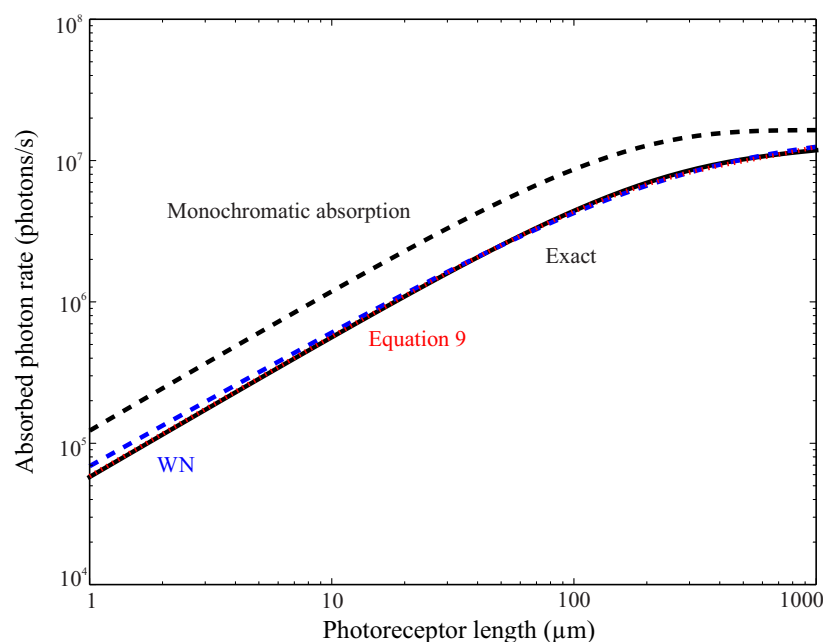
Figure 3. Absorption of blue skylight by UV rhodopsin as a function peak absorption coefficient *k* and photoreceptor length *l*, $F_a(kl)$. The exact calculation (black solid line) is very different from exponential absorption at the peak wavelength (black dashed line). The approximation to $F_a(kl)$ we used (red dotted line) fits better at very short lengths than approximation made by Warrant and Nilsson (1998) (blue dashed line) . Parameters used for calculations as in subscript to Figure 2 and Table 1.

Absorption rates in a tiered rhabdom with non monochromatic light

To calculate the correct versions of Equations 5 and 6 for blue skylight, it is easier to consider transmittances, the fraction of photons transmitted by each photoreceptor, R7 and R8, in the tiered configuration. We will denote these coefficients, a_7 and a_8 for light polarized in each photoreceptor preferred direction of absorption, and b_7 and b_8 for the perpendicular directions. In terms of these coefficients, which depend on the length of the photoreceptors and the wavelength content of the light, absorption in R7 and R8 can be written as:

$$N_7 = (1 - a_7)N_\parallel + (1 - b_7)N_\perp \tag{10a}$$

$$N_8 = (1 - b_8)a_7 N_\parallel + (1 - a_8)b_7 N_\perp \tag{10b}$$

The fraction of photons transmitted by the central rhabdom (the product of the fraction of photons transmitted by R7 and R8) to light polarized at $0°$ is:

$$a_7 b_8 = \int e^{-k_\parallel(\lambda)l_7} e^{-k_\perp(\lambda)l_8} I_\lambda(\lambda)d\lambda = 1 - F_a(k_\parallel l_7 + k_\perp l_8) \tag{11}$$

where l_8 is the length of R8. The fraction absorbed in R8 is the difference between light transmitted by the rhabdom and light transmitted by R7:

$$(1 - b_8)a_7 = (1 - a_7 b_8) - (1 - a_7) = F_a(k_\parallel l_7 + k_\perp l_8) - F_a(k_\parallel l_7) \tag{12}$$

similarly, the fraction of photons polarized at $90°$ that are absorbed in R8 is

$$(1 - a_8)b_7 = (1 - b_7 a_8) - (1 - b_7) = F_a(k_\perp l_7 + k_\parallel l_8) - F_a(k_\perp l_7) \tag{13}$$

Substituting the expression for the fractions of photons absorbed ($1 - a_7$, $1 - b_7$, $(1 - b_8)a_7$ and $(1 - a_8)b_7$) in equation 10, we we obtain the absorption rates of N_7 and N_8 for any given rhabdomere lengths, l_7 and l_8:

$$N_7 = F_a(k_\parallel(\lambda_{max})l_7)N_\parallel + F_a(k_\perp(\lambda_{max})l_7)N_\perp \tag{14a}$$

$$N_8 = \left[F_a(k_\parallel(\lambda_{max})l_7 + k_\perp(\lambda_{max})l_8) - F_a(k_\parallel(\lambda_{max})l_7) \right] N_\parallel + \\ \left[F_a(k_\perp(\lambda_{max})l_7 + k_\parallel(\lambda_{max})l_8) - F_a(k_\perp(\lambda_{max})l_7) \right] N_\perp \tag{14b}$$

Polarization sensitivity, signal and noise

Transduction and absorption rates

Sensitivity, signal and noise depend upon the transduction rate M; the rate at which a photoreceptor transduces absorbed photons to quantum bumps (unitary electrical responses to single photons). At lower light levels (up to approximately 5×10^4 transduced photons s^{-1}, a fly photoreceptor transduces a constant high proportion (> 0.5) of absorbed photons (Dubs et al., 1981; Howard et al., 1987; van Steveninck and Laughlin, 1996a). For simplicity we assume that $M = N$. At higher light levels transduction units (microvilli) saturate and this reduces sensitivity, reduces signal and changes the statistics of noise (Howard et al., 1987; Song et al., 2012). To account for these effects we convert the absorption rate, N, to the transduction rate, M, using our transduction unit saturation model (see below).

Polarization sensitivity without transduction unit saturation

In the absence of transduction unit saturation, transduction rates N equal absorption rates M. Because the microvilli of R7 and R8 are well aligned, the polarization angles at which transduction rates are maximum and minimum, θ_{max} and θ_{min}, are parallel and perpendicular to the microvilli, respectively. Thus $\theta_{min} = 90° + \theta_{max}$.

Polarization sensitivity is the ratio between the maximum and minimum transduction rates produced by linearly polarized light (degree of polarization $d = 1$) of constant intensity (Snyder, 1973):

7/33

$$PS = \frac{M(\theta_{\max}, d=1)}{M(\theta_{\min}, d=1)} \tag{15}$$

153 Note that for simplicity we present generic equations in which M stands for either M_7 or M_8, depending
154 on whether it is calculated using N_7 or N_8.

155 ### *Signal, noise and contrast; unsaturated regime*

156 To calculate signal and noise, we follow opponent models of color coding (Osorio and Vorobyev, 1996;
157 Vorobyev and Osorio, 1998), and normalise photon transduction rate, $M(\theta)$, to the background rate, M_{bg}

$$q(\theta) = \frac{M(\theta)}{M_{\mathrm{bg}}} \tag{16}$$

158 The background is unpolarized light with the same spectrum and intensity, N_i. We take M_{bg} to be the
159 mean transduction rate, in which case $q(\theta)$ is a contrast signal.

160   Given a constant photon flux N_i with polarization degree d, the transduction rate $M(\theta)$, and hence the
161 contrast signal $q(\theta)$, varies with the polarization angle θ as $\cos(2\theta)$ or, equivalently, $\cos^2(\theta)$.

$$q(\theta) = 1 + d\frac{PS-1}{PS+1}\cos 2(\theta - \theta_{\max}) \tag{17}$$

162 Note that the background ($d=0$) produces the same quantum catch as light polarized at $45°$ to the
163 preferred absorption axis ($\theta_{\max} = 45°$).

164   The range of contrast signals produced by changes in polarization angle, Δq, depends on the degree of
165 polarization, d, and the PS given by equation 17 :

$$\Delta q = q(\theta_{\max}) - q(\theta_{\min}) = 2d\frac{PS-1}{PS+1} \tag{18}$$

166   The reliability of an optical signal is limited by photon noise, random fluctuations in absorption rate
167 that follow the Poisson distribution. In the absence of transduction unit saturation we assume that every
168 absorbed photon produces a quantum bump. Thus during a time interval τ, a photoreceptor transduces
169 $\mathbf{M}^{(\tau)}(\theta)$ photons, drawn from a Poisson distribution with mean $M^{(\tau)}(\theta) = \tau M(\theta)$. By definition, the
170 noise variance equals the mean:

$$\mathrm{Var}(\mathbf{M}^{(\tau)}(\theta)) = \langle \mathbf{M}^{(\tau)}(\theta) \rangle = \tau M(\theta) \tag{19}$$

171 Note that randomly fluctuating variables are in bold.

172   We define the signal to noise ratio, SNR, as the ratio between the range of signals produced by changes
173 in polarization angle and the standard deviation of photon noise. This definition holds for both quantum
174 catches $\Delta M^{(\tau)}$ and contrast signals Δq:

$$SNR = \frac{\Delta M^{(\tau)}}{\sqrt{\mathrm{Var}(\mathbf{M}^{(\tau)}(\theta))}} = \frac{\Delta q}{\sqrt{\mathrm{Var}(\mathbf{q}^{(\tau)}(\theta))}} \tag{20}$$

175   Assuming that photon noise is independent of the contrast signal

$$SNR = \frac{\Delta q}{1/\sqrt{\tau M_{\mathrm{bg}}}} = 2d\frac{PS-1}{PS+1}\sqrt{\tau M_{\mathrm{bg}}} \tag{21}$$

176 This assumption is valid for small contrast signals, as produced at low degrees of polarization, d.

Transduction unit saturation, sensitivity, signal and noise

In fly photoreceptors each microvillus acts as a transduction unit, producing an all or nothing unitary response (a quantum bump) to the absorption of a single photon (Hardie and Raghu, 2001). To model the effects of transduction unit saturation we divide the rhabdomere into thin (1 μm) segments and use equation 14 to obtain the mean and variance of photon absorption in each segment. This accounts for the change in mean absorption rate along the rhabdomere —light entering all but the first section is filtered by the sections above it.

Saturation occurs because it takes time for a microvillus to reload after it produces a quantum bump. This dead time, t_d, sets the minimum interval between quantum bumps produced by a microvillus. Thus at high light levels a microvillus's transduction rate fails to keep up with its absorption rate. Consider a $0.5\,\mu m$ segment of rhadomere with n_m microvilli, absorbing an average of N_s photons per second. Photons are absorbed in each of the n_m microvilli with Poisson probabilities of parameter $N_s t_d / n_m$, but when more than one photon is absorbed in the time interval t_d, only one photon is transduced. As a consequence, during the interval of time t_d, each microvillus either transduces one photon with probability

$$\mathscr{P}(1) = 1 - e^{-\frac{t_d N_s}{n_m}} \tag{22}$$

or does not transduce it, with a probability

$$\mathscr{P}(0) = e^{-\frac{t_d N_s}{n_m}} \tag{23}$$

Considering the n_m microvilli in a single segment of rhabdomere, the number of photons transduced $\mathbf{M}^{(\tau)}$ during an integration time τ (which we take to be an integer multiple of t_d) follows a binomial distribution with success probability $1 - e^{-\frac{t_d N_s}{n_m}}$ and number of trials $n_m \tau / t_d$. This binomial has a mean

$$\langle \mathbf{M}^{(\tau)} \rangle = (1 - e^{-\frac{t_d N_s}{n_m}}) n_m \tau / t_d \tag{24}$$

and variance

$$\text{Var}(\mathbf{M}^{(\tau)}) = e^{-\frac{t_d N_s}{n_m}} (1 - e^{-\frac{t_d N_s}{n_m}}) n_m \tau / t_d \tag{25}$$

Note that at low light level, $N_s t_d / n_m \ll 1$ and our binomial model approximates the Poisson distribution of the absorbed photons, as expected because at low light levels the effects of saturation on signal and noise are negligible.

$$\langle \mathbf{M}^{(\tau)} \rangle = \text{Var}(\mathbf{M}^{(\tau)}) = N_s \tau \tag{26}$$

Because photons are transduced independently in each microvillus, and hence in every segment, the mean numbers of photons transduced by R7 and R8, $M_7^{(\tau)}$ and $M_8^{(\tau)}$, and their variances, can be obtained by summing the means and variances of all segments.

Polarization opponent model

To assess the effects of signal and noise on the ability to discriminate angles of polarization, we consider the output of a simple opponent mechanism that subtracts the input from R8 from the input from R7 in the same ommatidium. The opponent unit's output $\mathbf{Q}^{(\tau)}$ is the difference between the two photoreceptor contrast signals, q_7 and q_8:

$$\mathbf{Q}^{(\tau)} = \mathbf{q_7}^{(\tau)} - \mathbf{q_8}^{(\tau)} = \mathbf{M_7}^{(\tau)}(\theta)/M_{7,\text{bg}}^{(\tau)} - \mathbf{M_8}^{(\tau)}(\theta)/M_{8,\text{bg}}^{(\tau)} \tag{27}$$

where q_7 and q_8 are calculated by replacing M with M_7 and M_8 respectively in equation 16.

$\mathbf{Q}^{(\tau)}$ is a random variable whose mean is independent of the integration time τ:

9/33

$$\langle \mathbf{Q}^{(\tau)} \rangle = M_7^{(\tau)}(\theta)/M_{7,\mathrm{bg}}^{(\tau)} - M_8^{(\tau)}(\theta)/M_{8,\mathrm{bg}}^{(\tau)} \tag{28}$$

$$= M_7(\theta)/M_{7,\mathrm{bg}} - M_8(\theta)/M_{8,\mathrm{bg}} \tag{29}$$

but has (noise) variance that depends on τ. The variance of $\mathbf{Q}^{(\tau)}$ will be the sum of noise variance incoming both R7 and R8, and intrinsic noise variance. Thus, in the absence of saturation

$$\mathrm{Var}(\mathbf{Q}^{(\tau)}) = \mathrm{Var}(\mathbf{q_7}^{(\tau)}) + \mathrm{Var}(\mathbf{q_8}^{(\tau)}) + 2(\sigma_{\mathrm{in}}^{(\tau)})^2 \tag{30}$$

$$= \left[M_7(\theta)/M_{7,\mathrm{bg}}^2 + M_8(\theta)/M_{8,\mathrm{bg}}^2 + 2\sigma_{\mathrm{in}}^2 \right]/\tau \tag{31}$$

where σ_{in}^2 and $(\sigma_{\mathrm{in}}^{(\tau)})^2$ are the variances of intrinsic noise (resulting from Gaussian white noise added to the contrast signal $\mathbf{q_7}$ and $\mathbf{q_8}$ of each of the photoreceptors) in a signal integrated across an interval of 1 s and an interval τ respectively.

Number of discriminable polarization angles: a measure of performance which considers noise

Photon noise and intrinsic noise limit how precisely the light polarization angle, θ, can be estimated. To quantify the effect, we take successful models in colour vision (Vorobyev and Osorio, 1998) as a basis, considering the R7/R8 system as equivalent to a dichromatic space. We defined a distance ΔS between the signals generated in the opponent unit by light partially polarized with the same degree of polarization d and photon flux N but with polarization angles θ_1 and θ_2:

$$\Delta S = \frac{|Q(\theta_1) - Q(\theta_2)|}{\sqrt{\mathrm{Var}(\mathbf{Q}^{(\tau)})}} = \frac{|[q_7(\theta_1) - q_7(\theta_2)] - [q_8(\theta_1) - q_8(\theta_2)]|}{\sqrt{\mathrm{Var}(\mathbf{q_7}^{(\tau)}) + \mathrm{Var}(\mathbf{q_8}^{(\tau)}) + 2(\sigma_{\mathrm{in}}^{(\tau)})^2}} \tag{32}$$

This distance depends both on the amount the opponent signal Q changes for different polarization angles —ultimately determined by the PS of R7 and R8 (Equation 18)— and the reliability of the opponent signal, i.e. the amount of noise (composed of intrinsic and photon noise). A change in polarization angle $\Delta\theta$ can be detected in the opponent signal when the distance ΔS is bigger than a given value. For simplicity, we will take this threshold to be 1, so ΔS, as defined in Equation 32, is directly the number of discriminable polarization angles between polarization angles θ_1 and θ_2.

When considering the number of discriminable polarization angles between angles that produce very different quantum catches, we need to take into account that the photoreceptor noise varies as one moves across the stimulus space. The stimulus space is thus endowed of a Riemannian metric (Wyszecki and Stiles, 1982). The distance between light polarized at 0 degrees and light polarized at 90 degrees following a path of constant degree of polarization is better approximated by (Osorio and Vorobyev, 1996):

$$\Delta S = \sum_{i=0}^{n-1} \frac{|[q_7(\theta_i) - q_7(\theta_{i+1})] - [q_8(\theta_i) - q_8(\theta_{i+1})]|}{\sqrt{\mathrm{Var}(\mathbf{q_7}^{(\tau)}(\theta_i)) + \mathrm{Var}(\mathbf{q_8}^{(\tau)}(\theta_i)) + 2(\sigma_{\mathrm{in}}^{(\tau)})^2}} \tag{33}$$

with $\theta_0 = 0 < \theta_1 < ... < \theta_{n-1} < \theta_n = 90$ degrees.

Mutual information: a different measure of performance

We use information theory to define a second measure of the ability to discriminate between different polarization angles. This new measure quantifies how much we can reduce our uncertainty on the polarization angle by a single measure of the noisy opponent signal. In principle, it should be related to, but does not necessarily correlate with, measures based on ideal observer performance, such as the total number of discriminable angles (Thomson and Kristan, 2005).

Let $\theta \in [0, \pi/2)$ be the polarization angle, $\mathbf{Q}$ the signal of a polarization-opponent unit, and $f(\theta), f(Q)$ and $f(Q, \theta)$ their marginal and joint probability density functions. We assume that the distribution of polarization angles θ is uniform, i.e. $f(\theta) = 2/\pi$, and that the degree of polarization d is constant.

10/33

If there was no noise, $\mathbf{Q}$ would be simply a function of θ, $Q(\theta)$. Since the system is limited by noise, we consider the probability density of $\mathbf{Q}$ when we know θ. Under reasonable assumption it is a Gaussian of standard deviation $\sigma_Q = \sqrt{\mathrm{Var}(\mathbf{Q})}$, in our case a function of the angle of polarization θ:

$$f(Q|\theta) = \frac{1}{\sigma_Q(\theta)\sqrt{2\pi}} e^{\frac{-(Q-Q(\theta))^2}{2\sigma_Q^2(\theta)}} \tag{34}$$

$$\sigma_Q^2(\theta) = (M_7(\theta)/M_{7,\mathrm{bg}}^2 + M_8(\theta)/M_{8,\mathrm{bg}}^2 + 2\sigma_{\mathrm{in}})/\tau \tag{35}$$

The mutual information or rate of transmission of information between the two continuous random variables θ and $\mathbf{Q}$ is then defined as (Shannon, 1948)

$$I(\mathbf{Q};\theta) = \int\int f(Q,\theta) \log\frac{f(Q,\theta)}{f(\theta)f(Q)} d\theta dQ \tag{36}$$

which quantifies how much a measure of the opponent signal, Q, reduces the uncertainty about the polarization angle, θ, assuming that we are certain about the degree of polarization, d.

Choice of parameters

Measurements suggest that the absorption coefficient of a photoreceptor rhabdomere for unpolarized light ($\frac{k_\parallel + k_\perp}{2}$) lies between $0.01\mu m^{-1}$ (e.g. Hardie 1984) and $0.005\mu m^{-1}$ (Warrant and Nilsson, 1998), so we took $k = 0.0075\mu m^{-1}$. Measurements of R7/R8 photoreceptors' PS in the DRA of *C. vicina* range from 6 to 19 (Hardie, 1984), so we chose a dichroic ratio of $\delta = \frac{k_\parallel}{k_\perp} = 10$. Sky has a maximum polarization degree of about $d = 0.6 - 0.8$ in the UV, at 90 degrees from the sun in clear skies, but smaller at other orientations and under different meteorological conditions (Barta and Horváth, 2004). Behavioural threshold was measured to be at a degree of polarisarion of $d = 0.05$ in crickets and $d = 0.1$ in honeybees (Barta and Horváth, 2004). In this chapter, we modelled a polarization degree of $d = 0.1$.

Blowfly R1-6 photoreceptors have around 9×10^4 microvilli along an average length of $250\,\mu m$ (Hardie, 1985; Hochstrate and Hamdorf, 1990). We assumed here a similar linear density of microvilli in the R7 and R8 of the DRA. We chose $t_d = 30ms$ for the minimum interval between transduced photons in a *C. vicina* microvilli (Hochstrate and Hamdorf, 1990; Song et al., 2012), and we assumed that the fly integrates the signal across three of those intervals, i.e. integration time $\tau = 90$ ms.

RESULTS

The division of the central rhabdom length

In the fly dorsal rim, the two polarization coding photoreceptors, R7 and R8, construct a rhabdom whose length, L, is of the order of $100\,\mu m$. R7 and R8 divide the rhabdom between them; R7 constructs the upper part, of length l_7 and R8 the lower of length l_8 (Figure 1). To see how the division of the rhabdom between R7 and R8 determines their ability to code polarization we model three determinants of signal quality, polarization sensitivity, polarization signal and signal to noise ratio as a function of their length fractions,

$$\hat{l}_7 = l_7/L \tag{37}$$

$$\hat{l}_8 = l_8/L \tag{38}$$

where $L = 100\,\mu m$.

The flux of available photons

Because photoreceptor signal and noise depend upon the numbers of photons absorbed and transduced, we start by establishing the numbers of photons available for absorption. Our optical model calculates the rate at which the facet lens delivers photons from a clear blue sky to the entrance aperture of R7's rhabdomere (Figure 1; Equations 1, 2). The model takes into account the intensity and wavelength spectrum of skylight, light gathering by the facet lens, rhabdomere diameter, and the spectral sensitivity

of R7 and R8's UV rhodopsin. The light flux at R7's entrance aperture, N_i, is given in terms of available photons. These are photons that have a significant chance of being absorbed by the UV rhodopsin —peak 335 nm (Hardie, 1984; Stavenga et al., 1993)— and have wavelengths between 300 nm and 413 nm.

We use the flux of available photons, N_i, as our measure of the intensity of incident light. At noon on a bright summer's day, when the light intensity is approximately 10^5 lux, $N_i = 1.6 \times 10^7$ photons s^{-1} (Methods 2.1). The lowest intensity we model, $N_i = 100$ photons s^{-1}, corresponds to late nautical twilight (Johnsen, 2012).

Polarization sensitivity and the length fractions of R7 and R8

When a photoreceptor is sensitive to the plane of linearly polarized light, absorption varies with the polarization angle, θ. Polarization sensitivity is defined as the ratio between the maximum absorption, at polarization angle $\theta_{\max}$ and the minimum absorption at $\theta_{\min}$, when illuminated with a constant and completely polarized light. In a rhabdomere that does not twist (as in the DRA), $\theta_{\max}$ is parallel to the rhabdomere's microvilli, and $\theta_{\min}$ perpendicular.

We use our optical model and our model of transduction unit saturation to show how the *PS*'s of R7 and R8 depend on length fraction. The optical model calculates the rates at which R7 and R8 absorb photons as a function of the polarization angle, $N_7(\theta)$ and $N_8(\theta)$, given available photons, N_i, with a degree of polarization, d (Equation 14). The model takes into account the known absorption properties of R7 and R8, their lengths and hence length fractions, and the filtering by R7 of the light delivered to R8. *PS* is usually taken to be the ratio between maximum and minimum absorption rates, $N(\theta_{max})/N(\theta_{min})$ (e.g. Snyder 1973), but we go one step further.

We convert absorption rate, N, to a measure that is more closely related to a photoreceptor's ability to code information. the photon transduction rate, M. For a fly photoreceptor M is the rate at which it generates elementary electrical responses to single photons — quantum bumps. Below $M = 10^4$ photons s^{-1} the quantum efficiency of fly phototransduction is high, > 0.5, and constant (Methods; Dubs et al. 1981; van Steveninck and Laughlin 1996b). In this case we assume that the quantum efficiency of transduction = 1, therefore $M = N$. At higher light levels the transduction units that generate quantum bumps (individual microvilli) saturate. Saturation lowers the quantum efficiency of transduction so that M is significantly less than N, reduces signal amplitude and changes the statistics of noise (Howard et al., 1987; Song et al., 2012). We account for these effects with our transduction unit saturation model. By comparing results obtained with and without saturation we establish the low intensity regime in which saturation is negligible, and demonstrate the effects of saturation at higher light levels.

Our model confirms that the polarization sensitivities of R7 and R8, PS_7 and PS_8, are strongly dependent on the division of resources between R7 and R8 (Snyder, 1973). As the length fraction of $\hat{l_8}$ decreases, PS_8 increases because a longer R7 is a more effective polarization filter, and PS_7 decreases because the effects of self-screening increases with length. Thus for a central rhabdom of length $L = 100 \, \mu m$, PS_7 drops from its dichroic ratio, $\delta = 10$, to 7 and PS_8 increases from 7 to 24 (Figure 4i).

PS_7 and PS_8 are also sensitive to the spectrum of incident light. When illuminated with monochromatic light at peak absorption wavelength, 330 nm, R7 absorbs a higher fraction of incident photons. Consequently PS_7 is reduced more by self-screening, and PS_8 is increased more by filtering by R7. For example, when $L = 100 \, \mu m$ and $\hat{l_8} = 0.5$, $PS_7 = 7.5$ and $PS_8 = 13.9$. When $\hat{l_8}$ is vanishingly small, $PS_8 = 34$, more than three times the dichroic ratio. Irrespective of wavelength composition, these results show that to maximise PS almost all of the central rhabdom should be allocated to R7, and R8 should be vanishingly small.

Transduction unit saturation is significant above $N_i = 10^4$ photons s^{-1}, depressing PS_7 and PS_8 at all length fractions. This result suggests that saturation should be avoided by using the fly's longitudinal pupil (a dense array of small pigment granules that are drawn close to the rhabdomere in bright light) to attenuate the rhabdomeric photon flux (Anderson and Laughlin, 2000).

The dependence of polarization signal amplitude on the length fractions of R7 and R8

Signal amplitude depends upon $M(\theta)$, the relationship between transduction rate and polarization angle. To derive a signal that depends on polarization that is independent of background intensity we follow studies of colour coding (e.g. Vorobyev and Osorio 1998). $M(\theta)$ is normalized by dividing by the mean transduction rate M_{bg} to generate a contrast signal, $q(\theta)$. In the absence of saturation, $q(\theta)$ follows $\cos(2\theta)$, with an amplitude that increases linearly with the degree of polarization d and sub-linearly with PS (Equation 17);
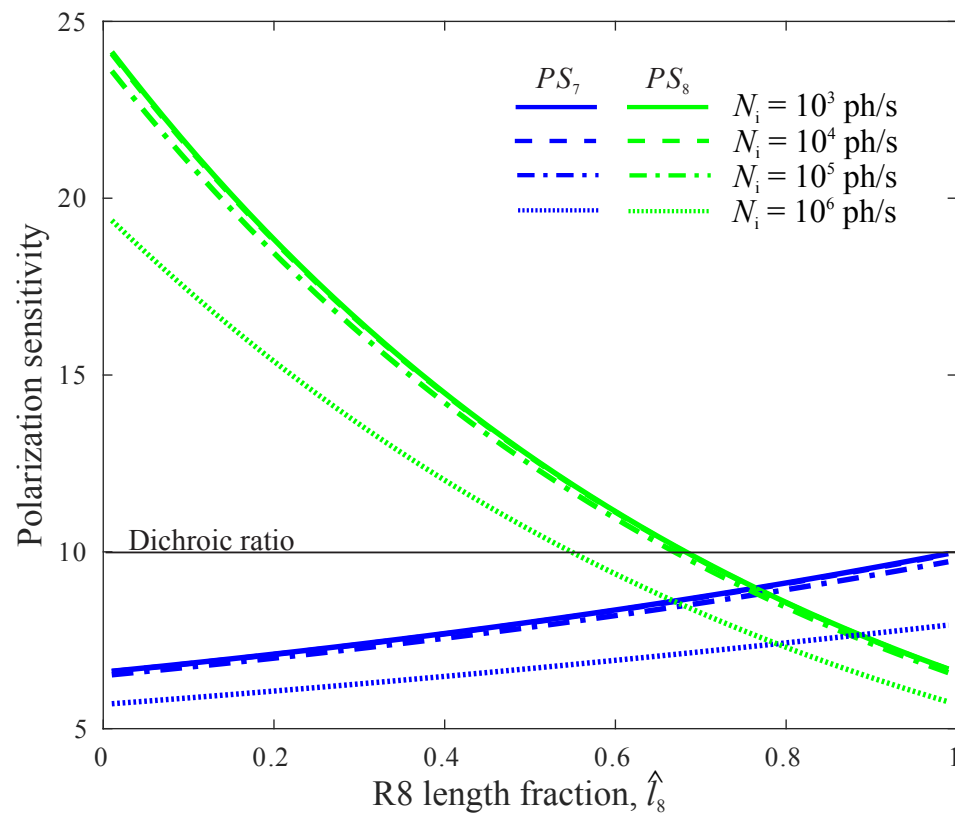
Figure 4. Polarization sensitivity of R7 and R8, PS_7 and PS_8, depends on division of rhabdom between R7 and R8, as specified by R8's length fraction $\hat{l}_8$. PS_7 and PS_8 do not vary with light level below $N = 1 \times 10^4\,ph/s$. Above this incident photon flux saturation reduces PS.

$$q(\theta) = 1 + d\,\frac{PS-1}{PS+1}\cos 2(\theta - \theta_{\mathrm{max}})$$

332   The range of contrast signals produced over all polarization angles is given by (Equation 18):

$$\Delta q = q(\theta_{\mathrm{max}}) - q(\theta_{\mathrm{min}}) = 2d\,\frac{PS-1}{PS+1}$$

333   Note that both $q(\theta)$ and Δq increase linearly with the degree of polarization, d and, due to the definition
334   of PS, sub-linearly with PS. Consequently $q(\theta)$ only specifies θ when the degree of polarization, d is
335   constant (Bernard and Wehner, 1977; How and Marshall, 2014), and the high values of PS_8 that are
336   produced by having a short R8 and long R7 have relatively little effect on q_8 and Δq_8. Indeed, as we will
337   now see, a short R8 is disadvantageous because it suffers badly from photon noise.

Photon noise, signal to noise ratio and the lengths fractions of R7 and R8

339   Photon noise, an inevitable consequence of photon absorption, limits the resolution of photoreceptor
340   signals. To calculate photon noise we integrate the photon transduction rate, $M(\theta)$, over a integration
341   time τ to obtain a quantum catch $M^{(\tau)}(\theta)$. Because photon noise is Poisson, its variance equals the mean
342    $\tau M(\theta)$. The effect of noise on the resolution of signal depends on the signal to noise ratio, SNR. Taking
343   as signal Δq, we obtain (Methods; Equation 21)

$$SNR = \frac{\Delta q}{1/\sqrt{\tau M_{\mathrm{bg}}}} = 2d\,\frac{PS-1}{PS+1}\sqrt{\tau M_{\mathrm{bg}}}$$

344   We note (Methods) that the SNR calculated using contrast equals the SNR calculated using transduction
345   rate because, to convert to contrast, both signal and noise are divided by the same factor, M_{bg}.
346   Like Δq, SNR increases linearly with d and sub-linearly with the polarization sensitivity PS. Also,
347   as in many optical systems limited by photon noise, SNR increases as the square root of mean quantum
348   catch. Consequently SNR is sensitive to both background intensity and photoreceptor length.
349   Because of this length dependence, SNR_7 and SNR_8 change greatly with the division of the central
350   rhabdom. Increasing R7's length fraction $\hat{l}_7$ (i.e. decreasing $\hat{l}_8$ in Figure 5) increases SNR_7 as more
351   photons are caught. Thus a reduction of the effects of photon noise more than compensates for the
352   loss of PS_7, and hence signal Δq_7, across the entire length range. If R7 were to be extended beyond
353   the limit imposed by the DRA's central rhabdom, self-screening would come to dominate. Thus SNR_7
354   would peak and then decline. With a dichroic ratio $\delta = 10$ and a maximum absorption coefficient $k =$
355    $0.0075\,\mu\mathrm{m}^{-1}$, as indicated by measurements made on fly photoreceptors, this optimum SNR_7 would occur
356   when $l_7 = 200\,\mu\mathrm{m}$. Increasing R8's length fraction has a similar effect; SNR_8 increases with $\hat{l}_8$, although
357   with smaller slope. At most length fractions, filtering by R7 increases SNR_8 by a small amount. For
358   example, when the central rhabdom is equally divided, $\hat{l}_7 = \hat{l}_8 = 0.5$, SNR_8 is slightly greater than SNR_7.
359   Given the dramatic effect of R7 on PS_8, its small influence on SNR_8 is somewhat surprising, but it
360   is easily explained. Reducing $\hat{l}_8$ reduces R8's quantum catch in two ways. First a shorter R8 absorbs a
361   smaller proportion of the photons delivered by R7. Second, a longer R7 delivers fewer photons. Thus
362   photon catch trumps screening and the division of central rhabdom that maximises both SNR_7 and SNR_8
363   is close to equal (Figure 5). But to what extent would such a division improve the ability of R7 and R8 to
364   code stimuli that are differently polarized? To address this question we use a model of opponent coding.

An opponent coding model demonstrates optimum length fractions

366   In our model an opponent unit subtracts the input from R8 from the input from R7 to produce an output
367   signal Q. As in color opponent models (e.g. Osorio and Vorobyev 1996), the photoreceptor inputs
368   have been independently normalized by dividing by the mean and correspond to contrast (Equation 16).
369   The two previous models of polarization opponency convert to contrast by taking the logarithm of light
370   intensity, as do photoreceptors over most of their response range (Nilsson et al., 1987; How and Marshall,
371   2014).
372   The opponent unit's output signal is the unweighted difference:
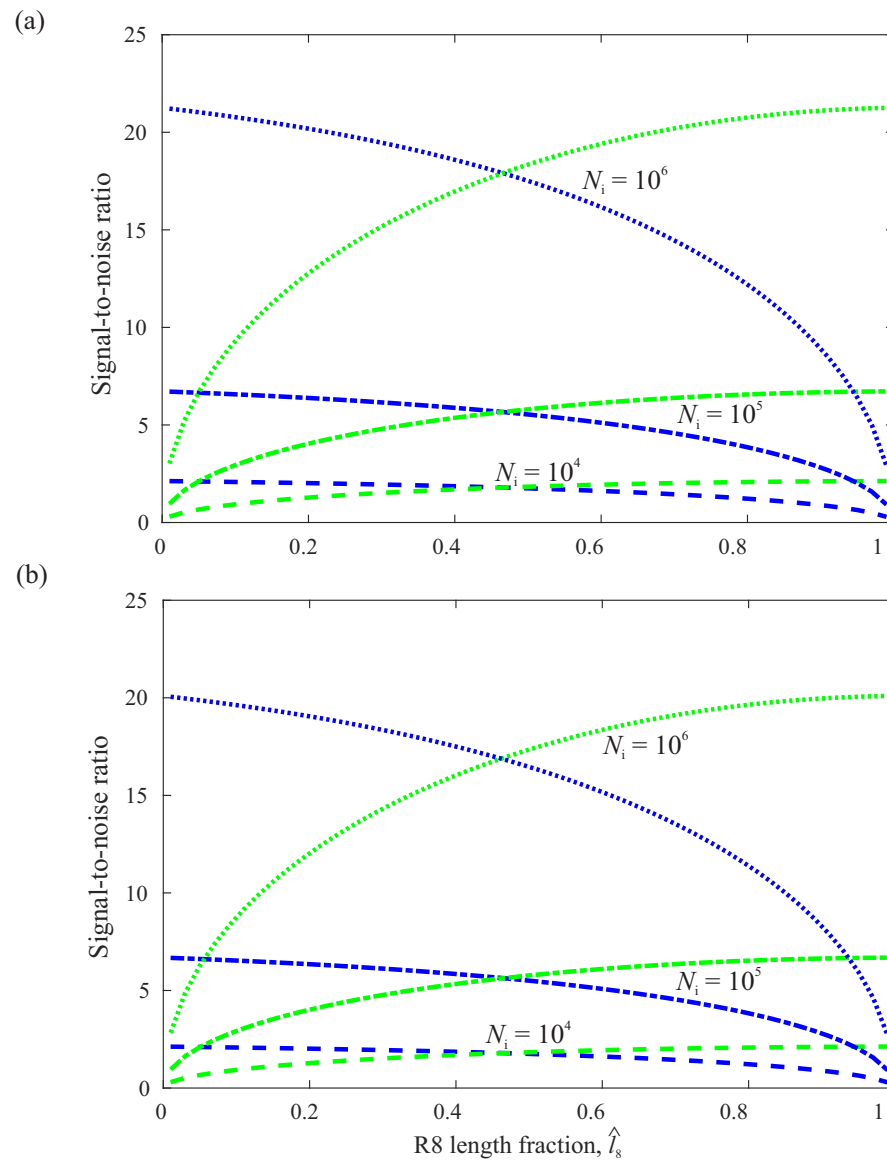
Figure 5. SNR in R7 (blue) and R8 (green) as a function of the fraction of the central rhabdom occupied by R8, $\hat{l}_8$, calculated for a rhabdom of fixed length $L = 100$ μm at three light levels, N_i. (a) calculated without modelling the saturation of transduction units; (b) calculated with saturation. Saturation reduces PS at the highest intensity.

$$Q(\theta) = q_7(\theta) - q_8(\theta) \tag{39}$$

where $q_7(\theta)$ and $q_8(\theta)$ are the contrast signals produced by R7 and R8 when they sample the same small patch of blue sky partially polarized at angle θ.

Just as we defined signal ranges for R7 and R8, the opponent signal range, ΔQ, is given by

$$\Delta Q = \max_{\theta}[Q] - \min_{\theta}[Q] = \Delta q_7 + \Delta q_8 \tag{40}$$
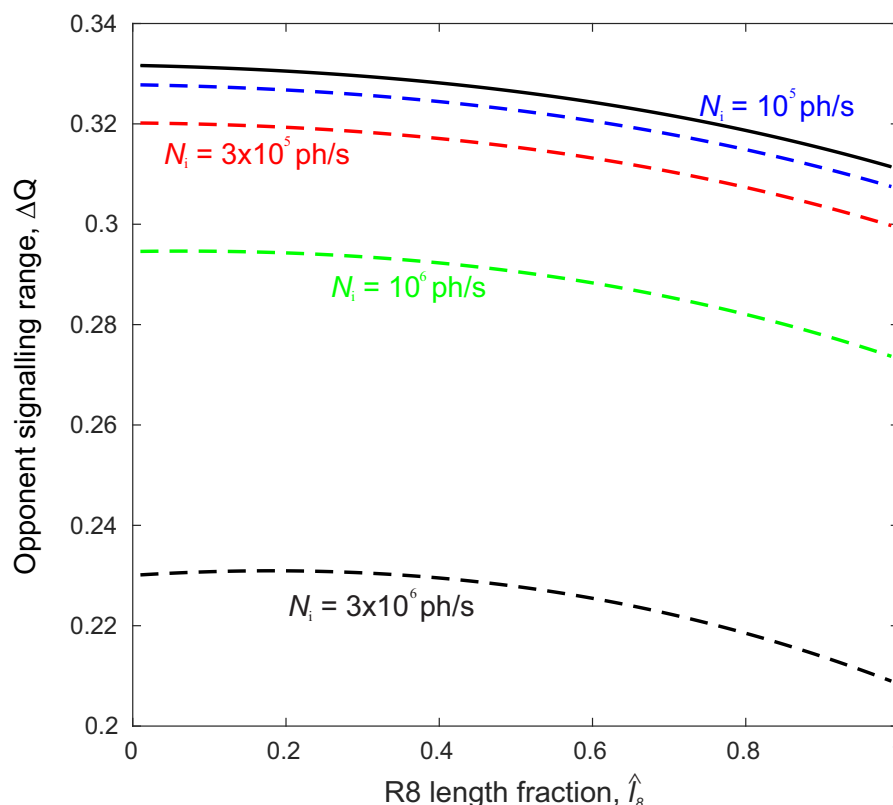
Figure 6. Polarization-opponent unit's signal range, ΔQ, is largest when the R8 length fraction, $\hat{l}_8$, is vanishingly small and, without transduction unit saturation (solid curves) does not depend on incident photon flux, N_i. Saturation progressively decreases ΔQ with increasing N_i (dashed curves). Rhabdom length, $L = 100$ μm. Incident photon flux, N_i: 1×10^5 (blue), 3×10^5 (red), 1×10^6 (green) and 3×10^6 (black) photons s^{-1}.

Recall that Δq_7 and Δq_8 depend on PS_7 and PS_8 (Equation 18) which in turn depend upon the length fraction $\hat{l}_8$ (Figure 4). It follows that ΔQ also varies with length fraction (Figure 6).

ΔQ is largest for a vanishingly small length fraction, $\hat{l}_8 \ll 1$ (Figure 6), mainly because PS_8 is maximum. However, although PS_8 changes four-fold with $\hat{l}_8$, (Figure 4) ΔQ changes by $< 7\%$ (Figure 6). This is because the photoreceptor signal range Δq depends on PS via the factor $\frac{PS-1}{PS+1}$ (Equation 18), which grows very slowly with PS at the higher values measured in photoreceptors, 6 to 19. Without saturation, ΔQ is independent of the photon flux N. Saturation takes effect at intensities in excess of $N_i = 10^5$ photons s^{-1} and progressively reduces ΔQ by as much as 30%. Saturation also increases the optimum length fraction $\hat{l}_8$, although the optimum is very broad. In summary, the shortest possible R8

16/33

385 generally produces the largest opponent signal because it has the highest *PS*. However, this configuration
386 is useless. The shortest R8 transduces so few photons that its signal is all but obliterated by photon noise.
387 We must now consider how noise degrades signal in the opponent unit.

Photon and intrinsic noise limit the resolution of opponent signals

389 Opponent models of visual coding readily take account of two sources of noise, the photon noise produced
390 when photoreceptors transduce photons and the intrinsic noise produced by subsequent neural mechanisms
391 such as ion channels and synaptic vesicle release (Faisal et al., 2008). Indeed, intrinsic noise is routinely
392 represented in models of sensory discrimination for two reasons. Even when presented with noise free
393 inputs, a brain cannot discriminate between infinitely many stimuli and intrinsic noise accounts for
394 absolute thresholds.

395 In our opponent model we express intrinsic noise in terms of equivalent contrast, i.e. a random
396 fluctuation in photoreceptor contrast signal that replicates the effects of intrinsic noise at the opponent
397 unit output . This contrast-referred intrinsic noise is assumed to have a Gaussian distribution with zero
398 mean. We set its variance so that intrinsic noise dominates at high light levels and photon noise dominates
399 at lower light levels, as observed in neurons post-synaptic to blowfly photoreceptors, elsewhere in the
400 eye (Laughlin et al. 1987; Methods). Photon noise has already been calculated (Methods, Equation 25).
401 Without saturation it is Poisson and with saturation it is binomial (Howard et al., 1987).

402 The opponent unit combines noise from independent sources, photon noise from R7, photon noise
403 from R8, and intrinsic noise. Consequently noise variances add, even though signals subtract, giving a
404 total noise variance in the opponent output (Equation 30)

$$\mathrm{Var}(\mathbf{Q}^{(\tau)}) = \mathrm{Var}(\mathbf{q_7}^{(\tau)}) + \mathrm{Var}(\mathbf{q_8}^{(\tau)}) + 2(\sigma_{\mathrm{in}}^{(\tau)})^2$$
$$= \left[M_7(\theta)/M_{7,\mathrm{bg}}^2 + M_8(\theta)/M_{8,\mathrm{bg}}^2 + 2\sigma_{\mathrm{in}}^2 \right]/\tau$$

405 To see how photon and intrinsic noise determine the accuracy with which polarization angle can
406 be coded we calculate the just noticeable difference (jnd) $\delta\theta$, in polarization angle as a function of
407 polarization angle (How and Marshall, 2014). For simplicity, the difference $\delta\theta$ is taken to be "just
408 noticeable" when it produces a change in opponent signal that equals the standard deviation of the total
409 noise, photon plus intrinsic. Plotting the inverse of $\delta\theta$ gives the discriminability of polarization angle, as
410 a function of θ.

411 Discriminability is greatest around an angle of $\theta = 45°$ (Figure 7). Here both R7 and R8 have
412 their highest sensitivity to changes in θ because *PS* follows a $\cos^2$ function. Increasing the incident
413 photon flux N_i, improves discriminability around all polarization angles, but does not shift the angle of
414 maximum discriminability (Figure 7 a,b). Decreasing the length fraction of R8, $\hat{l}_8$, from 0.5 to 0.1 reduces
415 discriminability across all angles. It does it at all three background intensities, but the relative decrease in
416 discriminability is higher at the lower light levels. This observation confirms the importance of photon
417 noise in a short R8. Although shortening R8 increases PS_8, and hence its contrast signal q_8, the loss
418 of quantum catch reduces SNR_8 to such an extent that its reduces the reliability of the opponent output
419 (Figure 7 a,b). Transduction unit saturation reduces discriminability at the highest light levels (Figure 7
420 b).

Coding ability depends on the length fractions of R7 and R8

422 The output of the opponent unit, Q, gives us two more measures of R7 and R8's ability to code the
423 polarization of the small patch of skylight that is projected onto their rhabdom. The first measure is
424 the number of discriminable polarization angles coded by the opponent unit (Equation 33). The second
425 measure is the mutual information between polarization angle and opponent signal (Equation 36). Our
426 models demonstrate that both measures of coding ability depend upon the division of a resource, a central
427 rhabdom of length *L*, between R7 and R8. As above, the allocation of this resource is specified by the
428 length fraction $\hat{l}_8$.

Number of discriminable polarization angles varies with the length fractions of R7 and R8

430 We follow previous studies of the opponent coding of color (Osorio and Vorobyev, 1996; Vorobyev
431 and Osorio, 1998) and polarization (How and Marshall, 2014) and calculate the total number of output
432 jnd's across all polarization angles. Our calculation takes into account the fact that a photoreceptor's

433 quantum catch, and hence photon noise, changes with polarization angle (Methods). An opponent signal
434 generated by a pair of photoreceptors with orthogonal PS confounds polarization angle θ with degree of
435 polarization, d (Bernard and Wehner, 1977; How and Marshall, 2014). For simplicity and directness we
436 assume $d = 0.1$, thereby assigning all changes in opponent signal, ΔQ, to changes in θ.

437   The length fraction $\hat{l}_8$ that maximizes the number of discriminable polarization angles depends upon
438 the amplitudes of intrinsic noise and photon noise, and upon transduction unit saturation (Figure 8). In
439 the absence of intrinsic noise (Figure 8a), i.e. only photon noise, the number of discriminable polarization
440 angles is maximum when R7 and R8 have approximately equal lengths ($\hat{l}_8 \approx 0.5$), at all light levels. This
441 near equal division is optimal because SNR increases with photoreceptor length (Figure 5). There is a
442 slight bias towards a longer R7 because this increases PS_8. Transduction unit saturation does not change
443 this optimum (Figure 8a).

444   At low and intermediate light levels intrinsic noise has no effect on the optimum $\hat{l}_8$ (Figure 8b);
445 $N_i = 1 \times 10^5$) because photon noise dominates. Consequently the number of discriminable polarization
446 angles is only slightly depressed by intrinsic noise. As intensity increases further, intrinsic noise comes
447 to dominate. The number of discriminable polarization angles is reduced and becomes less sensitive to
448 changes in length fraction. As N_i increases from 1×10^5 to 3×10^6 photons s^{-1} the optimum $\hat{l}_8$ falls from
449 0.5 to 0.33 (Figure 8c). Now a shorter R8 is advantageous because when intrinsic noise dominates it is
450 important to have a larger signal, and hence the higher PS of a shorter R8 (Figure 6). Transduction unit
451 saturation reduces the number of discriminable polarization angles above $N_i = 10^5$ and slightly reduces
452 the optimum $\hat{l}_8$ (Figure 8c).

453   We note in passing that our models identify three other factors that decrease the optimum $\hat{l}_8$ at highest
454 light levels, albeit to much lesser extent (results not shown). These minor factors are increasing the
455 dichroic ratio δ, illuminating the rhabdom with monochromatic light at the peak absorption wavelength,
456 and —up to a point— increasing the rhabdom length, L. All three factors allow R7 to act as a stronger
457 filter, making it more worthwhile to increase $\hat{l}_7$ and reduce $\hat{l}_8$.

458   In summary, with a rhabdom length, $L = 100\,\mu$m the optimum division between R7 and R8 strongly
459 depends on two factors, the relative contributions of photon noise and intrinsic noise, and weakly on
460 transduction unit saturation. Both these factors are intensity dependent and both favor a shorter R8 in
461 bright light. Thus the optimum R8 length fraction, l_8, reduces from 0.5 at lower light levels to 0.33 in
462 bright light. This range is similar to the length fractions observed in the DRA's of different fly species; $\hat{l}_8$
463 = 0.57 to $\hat{l}_8$ = 0.37 (Table 1).

Mutual information and length fractions of R7 and R8

465 We devised (Methods) a second measure of coding ability, mutual information, to confirm the conclusions
466 drawn from numbers of discriminable polarization angles. Mutual information specifies the amount
467 by which the opponent signal decreases our uncertainty about polarization angle, in bits. The measure
468 assumes that the signal is obtained by integrating transduction rate over the integration time, that successive
469 signals are independent, polarization angle has *a priori* a flat probability distribution, and the degree of
470 polarization is known.

471   Mutual information depends on light intensity and the length fractions of R7 and R8 (not shown). The
472 R8 length fraction, $\hat{l}_8$, that maximizes the mutual information (Figure 8d) is almost indistinguishable from
473 the R8 length fraction maximizing the number of discriminable polarization angles, across different light
474 levels (Figure 8c). As expected, mutual information increases with light level. When coding with optimal
475 length fraction, at $N_i = 10^5$ photons s^{-1}, an opponent signal carries approximately 1.2 bits per integration
476 time. Without saturation, mutual information increases with light level and approaches a ceiling of 1.7 bits
477 per integration time, set by intrinsic noise. With saturation, mutual information increases with intensity to
478 a maximum of around 1.5 bits per integration time and then decreases (not shown).

Central rhabdom length and polarization coding

480 The central rhabdom formed by R7 and R8 in the DRA is $50 - 60\%$ shorter than in the rest of the eye; $L=$
481 90 -120 μm c.f. 240 μm (Wada, 1974a,b; Wunderer and Smola, 1982a). Could it be shorter because it is
482 uniquely specialized to code polarization? We used our optical and opponent models to see how two of our
483 measures of performance, the opponent signal range and the number of discriminable polarization angles,
484 change with central rhabdom length, L. We modeled a range of lengths that exhibits all relevant effects,
485 $L = 20 - 300\mu$m and, for simplicity, we kept the length fractions of R7 and R8 equal; i.e. $\hat{l}_8 = \hat{l}_7 = 0.5$.

Opponent signal range and total length of the central rhabdom

Without saturation, the opponent signal range, ΔQ, reduces slightly with increasing L (Figure 9a), because self-screening decreases PS. Any increase in PS_8 due to stronger filtering by R7 is too weak to compensate for the loss in PS_7 due to self-screening because, as observed above, the relationship between PS and signal range is non-linear and $PS_8 > PS_7$. Nonetheless, the increase in PS_8 lessens the overall effect of increasing L. ΔQ falls by less than 10 percent as L goes from $20 - 300\,\mu m$, irrespective of light intensity (Figure 9b).

Saturation reduces signal range at all L's, but the reduction becomes smaller as L increases (Figure 9a dashed curves). Saturation favors a longer rhabdom because as absorption decreases the photon flux along the rhabdomere, the proportion of unsaturated microvilli increases. Thus it is advantageous to increase L up to an optimum length, beyond which the benefits of relief from saturation are outweighed by losses from self-screening (Figure 9a). The benefits of a longer L increase with the severity of saturation, and hence with incident photon flux, N_i. Thus when $N_i = 1 \times 10^5$ photons s^{-1} there is a barely perceptible optimum at $L = 60\,\mu m$. The optimum length increases to $120\,\mu m$ at 3×10^5 photons s^{-1} and $240\,\mu m$ at 1×10^6 photons s^{-1}. With an incident flux $N_i = 3 \times 10^6$ photons s^{-1} no optimum is a reached within the length range $20 - 300\,\mu m$. Note that although transduction unit saturation produces optimum lengths that depend on intensity, rhabdomeres that suffer less from saturation have larger ΔQ's at all L's. Thus a longitudinal pupil mechanism, which reduces saturation by attenuating rhabdomeric photon flux at high light levels (Howard et al., 1987), will increase ΔQ.

In summary, increasing L at high intensities increases signal range ΔQ by reducing the loss in PS produced by transduction unit saturation. This increase in ΔQ follows the Law of Diminishing Returns, and is opposed by the effects of self-screening. At all but the highest intensity the length used in the DRA, $L = 100\,\mu m$, performs close to the optimum and extending to the length used in the rest of the eye. Even at the highest light level considered, $L = 240\,\mu m$ produces a very small improvement in signal range ($< 8\%$).

Number of discriminable polarization angles and total length of the central rhabdom

Our second measure of performance, the number of discriminable polarization angles, almost invariably increases with rhabdom length, L, according to the Law of Diminishing Returns. Both the magnitude of Returns and the rate at which they diminish depend strongly on two factors - the relative effects of photon noise and intrinsic noise, and transduction unit saturation.

In the absence of intrinsic noise, the number of discriminable polarization angles increases with length (Figure 9 c,d) according to the Law of Diminishing Returns. When the number of angles is normalized with respect to $L = 100\mu m$, its increase is remarkably consistent; at all intensities it increases roughly 3-fold (over our length range) along approximately the same curve (Figure 9 e,f, black lines). The number of discriminable angles is improving because SNR_7 and SNR_8 increase with length (e.g. Fig. 3) and the Law of Diminishing Returns is enforced by two non-linearities. SNR increases as the square root of quantum catch (the Square Root Law) and catch per unit length decreases exponentially with rhabdomere length (Equation 9). Although the decrease in ΔQ with length (Figure 9 a) also diminishes returns, its contribution is minor. Transduction unit saturation slightly alters the relationship between length and normalized performance by punishing the shortest rhabdomeres and rewarding the longer (Figure 9d).

Adding intrinsic noise changes the relationship between the number of discriminable polarization angles and rhabdom length, L, to a degree that depends upon the magnitude of photon noise relative to intrinsic noise, and hence quantum catch. When quantum catches are relatively low, as happens at all L's at lower intensities and with shorter L's at higher intensities, photon noise dominates and intrinsic noise has almost no effect. In this situation the curves relating performance to length with intrinsic noise are virtually identical to those without (compare blue curves in Figure 9 e and c). As quantum catch rises the effect of intrinsic noise increases and comes to dominate.

The increasing effects of intrinsic noise are most clearly seen in the normalized plots (Figure 9d,f). Without intrinsic noise, the number of discriminable polarization angles rises 35% when L is extended from $L = 100\,\mu m$ to $L = 300\,\mu m$, independently of the light level. At the lowest intensity ($N_i = 1 \times 10^5$ photons s^{-1}, blue curve) intrinsic noise has little effect in shorter central rhabdoms, but reduces the performance increase to 16% when increasing total rhamdom length to $300\,\mu m$. At the next highest intensity ($N_i = 3 \times 10^5$ photons s^{-1}, red curve) intrinsic noise has a larger effect, particularly at longer L's, where quantum catch is higher. Thus intrinsic noise reduces the growth in relative performance between $L = 100\,\mu m$ and $L = 300\,\mu m$ from 35% to 7%. At $N_i = 1 \times 10^6$ photons s^{-1} growth is about

541   1%. At $N_i = 3 \times 10^6$ photons s^{-1} there is almost no growth at all because, as shown in Figure 9a, the
542   curve is almost flat at $L = 100\,\mu\text{m}$, and hits the upper limit imposed by intrinsic noise at $L = 150\,\mu\text{m}$. The
543   steady decline in percentage improvement noted above shows that as intensity increases, performance
544   approaches the intrinsic noise limit asymptotically. Transduction unit saturation decreases the total number
545   of distinguishable angles (Figure 9c,e) both with and without intrinsic noise and, as explained above,
546   favors longer rhabdoms (Figure 9d,f) because a smaller proportion of microvilli are saturated.

547   ***The DRA central rhabdom has an efficient length***

548   Our curves of performance (number of discriminable polarization angles) versus rhabdom length, L, allow
549   us to evaluate the benefits of extending the rhabdom from the length found in the DRA, $L = 100\,\mu\text{m}$
550   to the length found in the rest of the eye $L = 240\,\mu\text{m}$. These improvements compare with an increase
551   of 240% increases in the costs of space and materials allocated to the central photoreceptors, R7 and
552   R8. Elongation from $100\,\mu\text{m}$ to $100\,\mu\text{m}$ is of greatest benefit, 20%, at the lower light level $N_i = 1 \times 10^5$
553   photons/s. At higher light levels the benefit steadily reduces as photon noise becomes less important and
554   at $N_i = 3 \times 10^6$ photons/s there is no benefit without saturation. The rhabdom has hit the intrinsic noise
555   ceiling. With saturation the benefit is $< 10\%$.

556   Given that saturation happens, the best performance occurs at an incident photon flux, $N_i = 1 \times 10^6$
557   photons/s (green dashed curve in Figure 9e), in which case the benefit of extending from $100\,\mu\text{m}$ to
558    $240\,\mu\text{m}$ is $\approx 5\%$. Put differently, DRA's shorter central rhabdom increases the efficiency with which a
559   unit length of rhabdom codes the polarization of light at least two-fold. We conclude, therefore, that the
560   DRA's shorter central rhabdom is a specialization that promotes efficiency.

DISCUSSION

562   In the dorsal rim area of the fly compound eye, the DRA, photoreceptors R7 and R8 are specialized to
563   code the polarization of skylight. Because R7 and R8 form a tiered rhabdom with R7 placed in front
564   of R8 (Figure 1), R7 acts as a polarization filter that increases the polarization sensitivity of R8. We
565   demonstrate how his configuration sets up a trade-off between signal and noise. Lengthening R7, and
566   hence increasing its absorption, increases R8's polarization sensitivity and hence R8' signal. However,
567   lengthening R7 also reduces the number of photons R8 receives, thereby increasing the effect of photon
568   noise. We evaluate this trade off using a series of models, an optical model of photon absorption by R7
569   and R8, a model that accounts for the saturation of transduction units at high light levels, and an opponent
570   model of polarization coding that introduces intrinsic noise. We find that with a rhabdom of fixed length,
571   similar to that observed in the DRA, there are length fractions; i.e. divisions of the rhabdom between
572   R7 and R8, that optimize polarization coding by maximizing signal to noise ratio (SNR). Saturation of
573   transduction units at high intensities does not change these optimum length fractions, but reduces all
574   measures of performance. Furthermore an optimal optical configuration, namely photoreceptor length
575   fraction in a tiered rhabdom, depends in part on a neural factor, the level of intrinsic noise.

576   The intensity dependent range of optimum length fractions, 0.5 to 0.33 (Table 1), matches the range
577   of length fractions observed among flies, suggesting that R7 and R8 divide a resource, a central rhabdom
578   of given length, to optimize their ability to code polarization. Additional evidence for efficient resource
579   allocation is obtained by noting that in the DRA R7 and R8 make a central rhabdom that is shorter than
580   the peripheral rhabdomeres of photoreceptors R1-6, and 50% - 60% shorter than central rhabdomeres in
581   the rest of the eye. Our models show that this reduction in length doubles the efficiency with which the
582   DRA R7/R8 use rhabdom to code polarization, i.e. doubles the ratio between quantitative measures of
583   coding ability and rhabdom length.

584   We will now discuss the procedures we used, the validity of their assumptions, their relationship to
585   previous studies, and the novelty of their contributions. We will close by assessing the impact of our
586   findings on our understanding of the structure, function and design of photoreceptor arrays.

Modelling optical absorption

588   Our absorption model quantifies the optical trade-off between signal and noise by estimating the rates at
589   which the visual pigment molecules of photoreceptors R7 and R8 absorb photons when viewing a small
590   patch of polarized skylight. Our model confirms that optical effects within a rhabdom, namely filtering
591   and self-screening, play important roles in determining polarization sensitivity, as first demonstrated in the
592   central rhabdom of fly (Snyder, 1973; Gribakin and Govardovskii, 1975). We also confirm that, as shown

later in fused rhabdoms (Nilsson et al., 1987) and banded rhabdoms (Stowe, 1983), a photoreceptor's PS depends on its length, the orientation of its microvilli, the percentage of microvilli it contributes to the rhabdom, and the percentages and orientations of the microvilli of other photoreceptors that screen it. Filtering by a distal photoreceptor in a tiered rhabdom also sharpens and repositions the spectral absorption peaks of a proximal photoreceptor, as demonstrated in butterflies (Stavenga and Arikawa, 2006) and stomatopods (Marshall et al., 2007).However ours is the first study to investigate trade-off between signal and noise mediated by optical interactions within a fused rhabdom.

The trade-off between signal and noise set up by filtering has been demonstrated and analyzed in cone photoreceptors that place a coloured oil droplet in front of its visual pigment; i.e. in the cone inner segment, between the entrance aperture for light and the outer segment. The oil droplet sharpens the cone's spectral sensitivity by filtering the light delivered to the visual pigment, but also increases the effect of photon noise by reducing quantum catch. Our study of this optical trade-off is distinctive in two ways. The optical filter we consider is also a photoreceptor, R7, and this photoreceptor operates in tandem with the photoreceptor it shields, R8, to code a property of the light they sample, polarization.

To model absorption rates we make several simplifying assumptions. We assume that the dichroism produced by the alignment of rhodopsin molecules in microvilli is the only effect that changes the polarization of light as it travels down a rhabdomere. In fact, the rhabdomere is also optically anisotropic. However the resulting birefringence of a fly rhabdomere, $\Delta n < 1.0 \times 10^{-3}$ (Kirschfeld and Snyder, 1975; Beersma et al., 1982), produces a very small phase advance

$$\Delta\varphi = \frac{2\pi l \Delta n}{\lambda} < 1.13\,\mathrm{rad} \tag{41}$$

which in a rhabdomere of length $l = 60\,\mu\mathrm{m}$ is < 1.13 rad (41). Because this phase advance is equivalent to $< 18\%$ of a wavelength, it will have little effect on R7/R8 rhabdomeres in the DRA. Furthermore, optical experiments measured negligible birefringence in the longer DRA rhabdoms of ants (75-85 μm) and crickets (150-200 μm) (Nilsson et al., 1987). In even longer rhabdoms, birefingence can become important, producing mode beating between the polarized modes, as found in some butterflies (Nilsson et al., 1988). This beating reduces PS with increasing length, thereby accentuating the Law of Diminishing Returns that characterises the relationship between the coding ability of R7/R8 and central rhabdom length (Figure 9).

We calculated absorption at different wavelengths using a popular template for the spectral sensitivity of rhodopsins (Stavenga et al., 1993). This template provides an acceptable approximation of the absorption curve of a UV rhodopsin, although it slightly overestimates the curve's width (Stavenga, 2010). We disregard absorption by metarhodopsin because it absorbs in the blue, whereas almost all of the photons absorbed by the UV rhodopsin are at wavelengths below 413 nm, (Figure 2). Moreover, because daylight delivers more photons in the blue and the green, the rhodopsin:metarhodopsin ratio remains high in bright light. Consequently we can safely ignore the loss of sensitivity due to rhodopsin depletion.

We had to calculate the absorption of polarized skylight by UV rhodopsin, for a large number of combinations of rhabdomere length. To do this quickly and efficiently, we used the approach introduced by Warrant and Nilsson (1998). We fitted a convenient non-parametric function to a much smaller number of exact calculations of absorption, each made at a different length by integrating across all relevant wavelength. Although we use a different non-parametric function the calculations we make agree well with calculations made using Warrant and Nilsson's function for most photoreceptor lengths (Figure 3), with one small exception. Their function breaks down at very short lengths, where PS should equal the dichroic ratio. Alkaladi et al. (2013) adapted Warrant and Nilsson's approximation to analyse the PS of banded rhabdoms of the fiddler crab, and arrived at yet another expression, which is incompatible with the general expression for the absorption of polarized light in a tiered system (Equations 14). The mismatch arises because their derivation implicitly assumes that the light leaving each band has the same wavelength content as the light entering the photoreceptor from the facet lens.

Our findings rely on assumptions of homogeneity. Namely a rhabdomere's diameter and optical properties do not change with length and have R7 and R8 have identical, aside from their length and orientation of microvilli. The limited amount of physiological(Hardie, 1984) and anatomical (Wada, 1974a,b; Wunderer and Smola, 1982a) data does not indicate otherwise, with the exception that the cross-sectional area of R7's rhabdomere is on average 26% less than R8's in *Calliphora vicina* (Wunderer and Smola, 1982a).

21/33

645 There is no experimental data supporting the trade-off evaluated by our optical model. There are no
646 published measurements of photoreceptor noise in the fly DRA and the prediction that R8 has a higher
647 PS that R7 has not been reported (Hardie, 1984). Nonetheless there are several reasons to think that
648 our model is valid. The first is the small number of intracellular recordings from R8 photoreceptors in
649 the DRA. The second is the difficulty of making reliable recordings and measurements from such small
650 cells. The third is that when PS was measured it was done using 365 nm light (Hardie, 1984). At this
651 wavelength the UV rhodopsin's absorption is half maximal, which reduces the effect of filtering by R7 on
652 R8.

653 The most contentious assumption is that we ignore absorption by the longitudinal pupil; the pigment
654 granules that a photoreceptor moves close to its rhabdomere to attenuate bright light. Attenuation by the
655 pupil has not been measured in the DRA but in other eye regions the pupil "closes" progressively at high
656 intensites to attenuate the rhabdomeric photon flux by up to 2 log units. To a first approximation pupil
657 attenuation will be equivalent to reducing the incident photon flux, N_i. Although the pupil preferentially
658 absorbs longer wavelengths (Stavenga, 2004) this will have a small effect on the spectral sensitivities of
659 photoreceptors R7 and R8 in the DRA, because they absorb with a UV pigment. In any case, the pupil's
660 action will not alter the trade-offs and optimal length fractions we report. The pupil will simply extend the
661 range of incident photon fluxes at which these effects happen at the high intensities at which it operates.
662 In this extended range the effects of the pupil interacts with effects of transduction unit saturation photon
663 transduction rate, as discussed in the next section.

From photons absorbed to photons transduced

665 We converted photoreceptor absorption rates to transduction rates because the information photoreceptors
666 code depends upon the numbers of photons they transduce to electrical signals. Measurements of single
667 photon responses (quantum bumps) show that a single fly photoreceptor (type R1-6) transduces more
668 than 50% of photons arrive at lens, within its acceptance angle (Dubs et al., 1981). This means that well
669 over 50% of the photons arriving incident on its rhabdomere are transduced so, for simplicity, we assume
670 a quantum efficiency of 1. In this case the transduction rate equals the absorption rate. Noise analysis
671 shows that a fly R1-6 photoreceptor maintains its high quantum efficiency up to transduction rates of 10^4
672 photons/s (van Steveninck and Laughlin, 1996a). Above this intensity, quantum efficiency falls due to
673 the action of the longitudinal pupil (discussed above) and the saturation of transduction units (Howard
674 et al., 1987).

675 To account for the effects of transduction unit saturation on the mean and variance of transduction rate,
676 we extended the original binomial model (Howard et al., 1987) to take account of exponential absorption
677 along the rhabdom. Our improved model confirms that saturation had no effect on quantum efficiency,
678 and hence signal and noise, below rates of 10^4 photons/s and that above this it progressively reduces
679 signal and signal to noise ratio.

680 Basic binomial models simplify the causes and effects of transduction saturation. Do these simplifica-
681 tions invalidate our major conclusions? The binomial model assumes a dead time (refractory period) of
682 30 ms. The dead time has not been determined directly, however detailed, well-informed simulations of
683 the effects of transduction unit saturation (Song et al., 2012; Song and Juusola, 2014) suggest range of
684 mean values, from 10 ms to 100 ms, depending on fly species. Our value, 30 ms, is towards the lower
685 end of this range. Changing this value will not change the nature of the trade-offs, it will simply shift the
686 intensity range of saturation effects, according to the inverse of dead time.

687 A second simplification is that to calculate signal and noise, we sum transduction events (quantum
688 bumps) over a 90 ms time interval. However signals, absorption rates, quantum bump latencies, and
689 dead times vary continuously over time. Consequently the effects of transduction on signal and noise
690 depend upon time varying properties of signals and photoreceptor response dynamics. The detailed
691 simulations encapsulate these dynamics and show how they improve the coding of stimuli with natural
692 dynamics. These dynamic effects way well play a role in coding skylight polarization but, in the absence
693 of measurements of the natural time series of intensities experienced by R7 and R8 in the DRA, a detailed
694 simulation seems premature. Moreover incorporating the dynamics of signals, signalling and saturation
695 is unlikely to overturn our major conclusion that, given an optical signal, photon noise and intrinsic
696 noise there is an optimal division of rhabdom between R7 and R8. The optical trade-off between signal
697 and noise is based on fundamental principles and is little affected by transduction unit saturation. The
698 beneficial effects on coding documented by the more complicated models are largely due to changes in

22/33

quantum efficiency associated with large bursty contrast changes. They are not forthcoming in responses to stimuli that lack more prolonged dark contrasts (Song and Juusola, 2014), which may well be the stimuli coded by R7 and R8, because polarization and brightness change gradually and by relatively small amounts across a bright blue sky. The more complicated effects of saturation might come into play when the DRA of a rapidly turning fly views the sky through a broken canopy of vegetation.

Finally, both our model and the detailed simulations (Song et al., 2012; Song and Juusola, 2014) set aside the action of the longitudinal pupil. The pupil progressively attenuates the rhabdomeric photon flux to keep the transduction rate close to an experimentally demonstrated optimum, a peak in the contrast SNR that is captured by the binomial model (Howard et al., 1987). Our results concur (Figure 8). As intensity increases past the point at which saturation cuts in, discriminability continues to increase, but a declinig rate. It then reaches a peak falls by as much as 25% in brightest sunlight. This observation shows that a longitudinal pupil in the DRA's R7/R8 could usefully play the role advocated by Howard et al. (1987); limiting saturation so as to operate close to peak SNR. To determine the extent to which tranduction unit saturation changes the ability of a dorsal rim R7/R8 pair to code polarization, we must account for the pupil.

Opponent coding and discriminability

The use of an opponent model can be justified on several grounds (Hempel de Ibarra et al., 2014). First, neural processing involves opponent mechanisms. In color vision opponent mechanisms operate at the first stages of processing and at higher levels in both insects and vertebrates. In the polarization served by the DRA opponency has only been observed at higher levels. Second opponent processing provides a simple way to code a sub-modality, like color or polarization, independent of background intensity. Third, spatially and spectrally opponent mechanisms eliminate redundancy (Srinivasan et al., 1982; Buchsbaum and Gottschalk, 1983). Fourth, and most importantly for our purposes, opponent models of color vision account for exacting behavioral measures of discrimination (Hempel de Ibarra et al., 2014).

As in studies of color vision, we assess discriminability using an opponent model that scales and combines signals and noise (Hempel de Ibarra et al., 2014). An opponent unit takes the difference between the inputs from R7 and R8, scaled to represent contrast by dividing photon rates and counts by their means. R7 and R8's scaled signals subtract and, being uncorrelated, their scaled noise variances add. Then intrinsic noise is added to generate an opponent output. This intrinsic noise has a constant variance, independent of light level. The opponent output represents a combination of polarization angle and degree of polarization, and noise determines just noticeable differences in this combination. The jnd's define discriminability and the relationship between opponent signal and noise determines mutual information.

How and Marshall (2014) were the first to apply this approach to polarization vision. An earlier model (Nilsson et al., 1987) showed how a polarization-opponent signal is affected by an unequal share of microvilli directions in a fused rhabdom, but did not include noise. How and Marshall used their opponent model to show how under natural conditions the rhabdomeres in the fiddler crab are optimally oriented to detect the polarization degree rather than the polarization angle. To set the noise level they assumed a single source and adjusted its variance to account for jnd's in polarization, measured behaviourally. We independently applied their approach, and in doing so we extended it to separate the effects of intensity dependent photoreceptor noise (e.g. photon noise) and intrinsic noise.

Our estimates of discriminable angles and mutual information depend upon assumptions about integration time and intrinsic noise variance. The chosen integration time interval $\tau = 90$ ms, is arbitrary. It will affect the absolute values of SNR, numbers of angles and mutual information but not their relative values (e.g. Equation 20). Thus the shapes of curves relating performance to length and light level are the same and the optima are unchanged.

There are no measurements of intrinsic noise in the neural pathways served by the DRA so we chose an intrinsic noise variance ($\sigma_{in}^2 = 5 \times 10^{-5}$) that is about 7.5 times greater than photon noise at an incident photon flux of $N_i = 1 \times 10^6$ photons/s. This value is in accordance with measurements of noise in large monopolar cells (LMCs), directly post-synaptic to photoreceptors R1-6 (van Stevenink and Laughlin, 1996b). At medium frequencies, around 50 Hz, an LMC's intrinsic noise is 7 times that fed through from photoreceptors R1-6 and at high frequencies, around 100 Hz 10 times greater. Because the polarization signal changes gradually across the sky we favoured the lower value. The R1-6 axon terminals in the lamina form a massive parallel array of 1200 active zones driving each LMC (Nicol and Meinertzhagen, 1982; van Stevenink and Laughlin, 1996b). If such costly structure is not present in the R7/8 projection

to the medulla, intrinsic noise could well be larger.

The underestimate will not be huge —noise goes as the square root of the number of synapses. Nor will an underestimate change the nature of the trade-offs we describe and the optima they create. An increase in noise simply reduces the light intensity at which intrinsic noise starts to dominate photon noise, and this shifts the curve relating optimum R8 length fraction to light intensity to lower intensities. For example, if the number of release sites were reduced by 99% the intrinsic noise variance is ten times larger ($\sigma_{in}^2 = 5 \times 10^{-4}$), the optimum length fraction of R8 at $N = 1 \times 10^6$ photons/s drops to 0.25 and the Law of Diminishing Returns on central rhabdom length becomes more severe because performance approaches a lower intrinsic noise ceiling. In other words, higher levels of intrinsic noise favour shorter rhabdoms because they use the resource of rhabdom length more efficiently. We will return to this point in our final section.

Coding polarization signals from the dorsal rim area

No matter how they are processed, the signals coded by a pair of R7 and R8 cannot give unequivocal information about the polarization state of incoming light. Polarization angle is confounded by degree of polarization (Bernard and Wehner, 1977). Orientation cues are obtained from sky polarization patterns by integrating information from many central rhabdoms, each sampling a different patch of sky. Evidence from other insects, such as crickets, shows that higher order POL neurons integrate information from across the DRA, and suggests that they receive this information from small field opponent units, similar to the ones we model (Labhart, 1988; Labhart et al., 2001). Given the advantages of such an elementary opponent unit (see above), using it for the first stage in neural processing makes sense.

Our models could help understand how low intensity polarization patterns are resolved because they evaluate the effect of photon noise. This might help to explain how the DRA's of nocturnal beetles, and the neural pathways they serve, are adapted to support a remarkable behaviour - orientation to the polarization pattern of the night sky (Jundi et al., 2015). Our models evaluate the role of optics in determining ratios between polarization signal and photon noise and translate signal and noise into discrimination thresholds and mutual information, and this allows one to search for optimum sampling and processing strategies. Our modelling also takes account of the relative contributions of photon and intrinsic noise, which may be important because, when photoreceptor signals are pooled neutrally, the ratio between photon and intrinsic will decrease. In other words, we have done in theory what beetles may have done in practice, optimized the inevitable trade-off between polarization signal and noise within a constraint imposed by limited resources, in our case photoreceptor length.

The efficient use of photoreceptor length

Our study shows that photoreceptors R7 and R8 in the DRA are adapted to make efficient use of photoreceptor length. There are good reasons why both aspects of photoreceptor length, length of rhabdom and length of rhabdomere, should be allocated efficiently; length represents three limiting resources, materials, space and metabolic energy consumption, as follows. For a photoreceptor of given cross section, the consumption of space and materials increases in direct proportion to length. The relationship between energy consumption and length is less direct, but compelling. For a rhabdomere of given cross-section, the number of microvilli increases in proportion to length. More microvilli means a larger light-gated conductance, and to avoid saturation of membrane potential, a larger potassium conductance. These larger conductances carry larger currents which consume more energy (Howard et al., 1987), as demonstrated by comparing photoreceptors of different length (Niven et al., 2007). This length-dependent energy consumption is significant; direct measurements confirm that retinal photoreceptors account for 8% of a blowfly's resting oxygen consumption (Pangršič et al., 2005). Given such a high level of consumption, adaptations that improve photoreceptor energy efficiency should promote fitness. One these grounds we suggest that it is valid to treat photoreceptor length as a limiting resource, to be used efficiently.

We demonstrate two routes to efficiency. One is to divide the length of the central rhabdom between photoreceptors R7 and R8 so as to optimize two measures of coding ability, number of discriminable polarization angles and mutual information. The division made in the fly DRA is close to optimal, and there are reasons to suggest that central rhabdoms in the rest of the eye are divided likewise. In the rest of the eye there are spectrally distinct classes of central rhabdom, suitable for color vision (Wunderer and Smola, 1982b; Hardie, 1985). In *Calliphora vicina*, there are two spectral classes of central rhabdom, R7y/R8y and R7p/R8y, distributed randomly across the photoreceptor array. There are

also two morphological classes of R8 with different relative lengths that, on the basis of their relative frequencies, can be associated with the two spectral classes (Smola and Meffert, 1979; Wunderer and Smola, 1982b). In the light of our modelling of the DRA, this evidence suggests that the length fractions of R7 and R8 are allocated to increase the efficiency of color coding. There are two reasons why the R7p/R8p central rhabdom could benefit from a shorter R8, and hence longer R7. One is that, because the spectral sensitivity curves of R7p and R8p overlap more than the curves of R7y and R8y, the signal in R8p will benefit more from the sharpening of spectral sensitivity produced by a longer R7p. The other is that, because the spectral sensitivity curve of R7p is narrower than the curve of R7y, and centred in shorter wavelengths where fewer photons are available, a longer R7p is needed combat photon noise. Our model of polarization opponency could be obviously be adapted back to color opponency to test these hypotheses, but the results may well depend on assumptions about what a fly uses its spectral classes of photoreceptors for.

The second route to efficiency is to regulate rhabdom length. Our modelling shows how efficient usage of rhabdom length can explain why the central rhabdom in DRA is approximately half the length of both peripheral (R1-6) rhabdomeres in the DRA and central rhabdoms elsewhere in the eye. The DRA's shorter rhabdom is more efficient for coding polarization because the relationship between central rhabdom length and number of discriminable polarization angles follows the law of diminishing returns (Figure 9). This version of the law is seemingly inescapable because it is enforced by biophysical constraints on signal and noise. Quantum catch increases sub-linearly with rhabdomere length due to exponential absorption. (Equation 9), (Figure 3) and at lower light levels SNR increases as the square root of quantum. At the highest light levels another length dependent factor, number of available transduction units (i.e. microvilli) constrains signal and noise, and the maximum achievable SNR tends to increase as the square root of the total number of transduction units (Howard et al. 1987). Constrained by these factors, doubling the length of the DRA's central rhabdom to equal that in the rest of eye increases the number of discriminable polarization angles by less than 10%, but halves the efficiency with which R7 and R8 use rhabdom length to code polarization.

Our theoretical arguments add to a growing body of experimental evidence that the number of transduction units, and hence microvilli, are a limiting resource to be employed efficiently. This evidence has been obtained by comparing photoreceptors within a single retina, and in the retinas of different species. Within the blowfly retina, photoreceptors R7 and R1-6 increase their SNR's with light intensity, and in full daylight approach a maximum asymptotically. This maximum SNR is lower in R7 than in R1-6, in accordance with there being fewer microvilli in R7's shorter rhabdomere (Anderson and Laughlin, 2000). Comparing R1-6 in the same retina, SNRs in bright light and information rates correlate with the optical resolving power of the photoreceptor array, being higher in the frontal eye region, which samples more densely with narrower acceptance angles (Burton et al., 2001). This suggests that transduction units are allocated according to need.

Turning to comparisons among species, measurements made from homologous R1-6 photoreceptors in four species of fly of increasing size, show that SNRs, information rates and energy consumption are higher in longer photoreceptors, while efficiencies (bits coded per ATP consumed) are lower, according to the law of diminishing returns (Niven et al., 2007). Comparing two species of similar size, the predatory killer fly Coenesia supports faster and more acute vision than the fructivorous Drosophila. To support its behaviour *Coenesia* uses longer photoreceptors with more microvilli to achieve a higher SNR (Gonzalez-Bellido et al., 2011). Thus comparative studies argue strongly that photoreceptor length is a limiting resource that is applied efficiently, according to behavioural requirements and constraints imposed by biophysics the properties of natural signals (Sterling and Laughlin, 2015, Chapter 8).

Conclusion and outlook

Our study of the optimal allocation of photoreceptor length for opponent polarization coding confirms that having longer rhabdomeres with more microvilli improves vision by increasing the SNR at a given rate of incident photon flux. This increase is achieved in two ways. At low light levels increasing microvilli increases quantum catch, and in full daylight it increases the rate at which transduction units register photons. Thus the number of microvilli plays an important role in the function, design and evolution of compound eyes (Howard and Snyder, 1983). Future studies of the ways which in the optics of compound eyes, and especially tiered rhabdoms, are adapted to visual ecology should take account of the limitations on signal and noise imposed by numbers of microvilli and their lengths (Gonzalez-Bellido et al., 2011).

Table 1. Fraction of the DRA central rhabdom occupied by R8 in different species of Diptera.

Species	l_8/L	References
Rhagio scolopacea	0.42	(Wada, 1974a)
Leptempis	0.45	(Wada, 1974a)
Ceratitis capitata	0.37	(Wada, 1974a)
Drosophila melanogaster	0.49	(Wada, 1974a)
Scatophaga stercoraria	0.57	(Wada, 1974a)
Musca domestica	0.53	(Wada, 1974a)
Calliphora vicina	0.4, 0.44	(Wada, 1974a; Wunderer and Smola, 1982a)
Sarcophaga carnaria	0.43	(Wada, 1974a)
Zeuxia	0.48	(Wada, 1974a)
Lipoptena cervi	0.54	(Wada, 1974a)

Our study shows how this can be done with an opponent model. We suggest that a fertile new approach, namely modifying opponent coding models from colour vision in order to relate the coding and processing of polarization signals to behaviour (How and Marshall, 2014), could well bear even more fruit if, like our study and the colour opponent models that have gone before, one takes into account intensity dependent photoreceptor noise. It will be interesting to see if future applications confirm our finding that the optimal configuration of a photoreceptor array depends not just on optics and transduction rate, but on the intrinsic noise introduced during neural transmission and processing. If this proves to be the case, efficiency will be improved by matching the allocation of resources in one component of a system, optics, to the resources invested in other components, neural processing. This design strategy, matching the application of resources to components within a system to optimize overall performance, is commonly observed in neurons and neural circuits (Sterling and Laughlin, 2015). Here we have demonstrated how this self-same strategy can be implemented within a rhabdom, by allocating rhabdomere length to R7 and R8.

Competing interests

The authors declare there are no competing interests.

Author contributions

F.J.H.H. and S.B.L. conceived and designed the study. F.J.H.H. wrote the code and performed the analysis. F.J.H.H. and S.B.L. wrote the paper.

Data availability

Original codes used to produce the figures have been uploaded to *https://gitlab.com/fjhheras/optimizing_pol_2016.git*

ACKNOWLEDGEMENTS

The authors thank R.C. Hardie, K.D. Longden, J.E. Niven, D.G. Stavenga and M. Wicklein for discussions and feedback on previous versions of this manuscript.

REFERENCES

Alkaladi, A., How, M. J., and Zeil, J. (2013). Systematic variations in microvilli banding patterns along fiddler crab rhabdoms. *Journal of Comparative Physiology A*, 199(2):99–113.

Anderson, J. C. and Laughlin, S. B. (2000). Photoreceptor performance and the co-ordination of achromatic and chromatic inputs in the fly visual system. *Vision Research*, 40(1):13–31.

Barta, A. and Horváth, G. (2004). Why is it advantageous for animals to detect celestial polarization in the ultraviolet? Skylight polarization under clouds and canopies is strongest in the UV. *Journal of Theoretical Biology*, 226(4):429–437.

Table 2. Table of symbols

Symbol	Meaning	Units
D_r	Rhabdomere diameter	nm
d	Degree of polarization	
ΔS	Number of discriminable polarization angles	
δ	Dichroic ratio of the rhabdomere	
F	F-ratio of the facet lens	
$F_a(\kappa)$	Absorptance for wide spectrum light, where $\kappa = lk(\lambda_{\max})$ is the product of rhabdomere length and the peak absorption coefficient	
$I(Q;\theta)$	Mutual information between opponent signal and polarization angle	bits
$k_\parallel(\lambda)$	Absorption coefficient for light of wavelength λ polarized parallel to the microvilli	μm^{-1}
$k_\perp(\lambda)$	Absorption coefficient for light of wavelength λ polarized perpendicular to the microvilli	μm^{-1}
L	Total length of central rhabdom	μm
$L(\lambda)$	Spectral radiance	photons $sr^{-1} m^{-2} nm^{-1}$
l_7, l_8	Lengths of rhabdomeres of R7 and R8	μm
λ	Wavelength of light	nm
M_7, M_8	Transduction rates	photons s^{-1}
$M_7^{(\tau)}, M_8^{(\tau)}$	Photons transduced per integration time τ by R7 and R8	photons
$N_i(\lambda)$	Spectral photon flux incident at the distal extreme of R7	photons nm^{-1}
N_i	Photon flux incident at the distal extreme of R7	photons s^{-1}
N_s	Absorption rate in a small section of the photoreceptor	photons s^{-1}
N_7, N_8	Absorption rates in R7 and R8	photons s^{-1}
$N_7^{(\tau)}, N_8^{(\tau)}$	Photons absorbed per integration time τ by R7 and R8	photons
PS	Polarization sensitivity	
q, q_7, q_8	Contrast signal in a photoreceptor / R7 / R8	
Q	Opponent signal	
SNR	Signal-to-noise ratio	
σ_{in}	Standard deviation of intrinsic noise	
t_d	Photoreceptor dead time	ms
τ	Integration time	ms
θ	Polarization angle	rad

Beersma, D. G. M., Hoenders, B. J., Huiser, A. M. J., and Van Toorn, P. (1982). Refractive index of the fly rhabdomere. *Journal of the Optical Society of America*, 72(5):583–588.

Bernard, G. D. and Wehner, R. (1977). Functional similarities between polarization vision and color vision. *Vision Research*, 17(9):1019–1028.

Buchsbaum, G. and Gottschalk, A. (1983). Trichromacy, opponent colours coding and optimum colour information transmission in the retina. *Proceedings of the Royal Society of London B: Biological Sciences*, 220(1218):89–113.

Burton, B. G., Tatler, B. W., and Laughlin, S. B. (2001). Variations in photoreceptor response dynamics across the fly retina. *Journal of Neurophysiology*, 86(2):950–960.

Dubs, A., Laughlin, S. B., and Srinivasan, M. V. (1981). Single photon signals in fly photoreceptors and first order interneurones at behavioral threshold. *The Journal of Physiology*, 317:317–334.

Faisal, A. A., Selen, L. P. J., and Wolpert, D. M. (2008). Noise in the nervous system. *Nature Reviews Neuroscience*, 9(4):292–303.

Fortini, M. E. and Rubin, G. M. (1991). The optic lobe projection pattern of polarization-sensitive photoreceptor cells in *Drosophila melanogaster*. *Cell Tissue Research*, 265(1):185–191.

Gonzalez-Bellido, P. T., Wardill, T. J., and Juusola, M. (2011). Compound eyes and retinal information processing in miniature dipteran species match their specific ecological demands. *Proceedings of the National Academy of Sciences*, 108(10):4224–4229.

Gribakin, F. G. and Govardovskii, V. I. (1975). The role of the photoreceptor membrane in photoreceptor optics. In Snyder, A. W. and Menzel, R., editors, *Photoreceptor Optics*, pages 215–236. Springer Berlin Heidelberg.

Hardie, R. C. (1984). Properties of photoreceptors R7 and R8 in dorsal marginal ommatidia in the compound eyes of *Musca* and *Calliphora*. *Journal of Comparative Physiology*, 154(2):157–165.

Hardie, R. C. (1985). Functional organization of the fly retina. In Autrum, H., Ottoson, D., Perl, E. R., Schmidt, R. F., Shimazu, H., and Willis, W. D., editors, *Progress in Sensory Physiology*, number 5 in Progress in Sensory Physiology, pages 1–79. Springer Berlin Heidelberg.

Hardie, R. C. and Kirschfeld, K. (1983). Ultraviolet sensitivity of fly photoreceptors R7 and R8: Evidence for a sensitising function. *Biophysics of structure and mechanism*, 9(3):171–180.

Hardie, R. C. and Raghu, P. (2001). Visual transduction in *Drosophila*. *Nature*, 413(6852):186–193.

Hempel de Ibarra, N., Vorobyev, M., and Menzel, R. (2014). Mechanisms, functions and ecology of colour vision in the honeybee. *Journal of Comparative Physiology A*, 200(6):411–433.

Hochstrate, P. and Hamdorf, K. (1990). Microvillar components of light adaptation in blowflies. *The Journal of General Physiology*, 95(5):891–910.

How, M. J. and Marshall, N. J. (2014). Polarization distance: a framework for modelling object detection by polarization vision systems. *Proceedings of the Royal Society B*, 281(1776):20131632.

Howard, J., Blakeslee, B., and Laughlin, S. B. (1987). The intracellular pupil mechanism and photoreceptor signal: Noise ratios in the fly *Lucilia cuprina*. *Proceedings of the Royal Society of London. Series B, Biological Sciences*, 231(1265):415–435.

Howard, J. and Snyder, A. W. (1983). Transduction as a limitation on compound eye function and design. *Proceedings of the Royal Society of London B*, 217(1208):287–307.

Johnsen, S. (2012). *The Optics of Life*. Princeton University Press, Princeton NJ.

Jundi, B. e., Warrant, E. J., Byrne, M. J., Khaldy, L., Baird, E., Smolka, J., and Dacke, M. (2015). Neural coding underlying the cue preference for celestial orientation. *Proceedings of the National Academy of Sciences*, 112(36):11395–11400.

Kirschfeld, K. and Snyder, A. W. (1975). Waveguide mode effects, birefringence and dichroism in fly photoreceptors. In Snyder, A. W. and Menzel, R., editors, *Photoreceptor Optics*, pages 56–77. Springer Berlin Heidelberg.

Kok, C. J. (1972). Spectral irradiance of daylight at Pretoria. *Journal of Physics D: Applied Physics*, 5(8):1513–1520.

Labhart, T. (1988). Polarization-opponent interneurons in the insect visual system. *Nature*, 331(6155):435–437.

Labhart, T. (2000). Polarization-sensitive interneurons in the optic lobe of the desert ant *Cataglyphis bicolor*. *Naturwissenschaften*, 87(3):133–136.

Labhart, T. and Meyer, E. P. (1999). Detectors for polarized skylight in insects: a survey of ommatidial specializations in the dorsal rim area of the compound eye. *Microscopy Research and Technique*,

47(6):368–379.

Labhart, T., Petzold, J., and Helbling, H. (2001). Spatial integration in polarization-sensitive interneurones of crickets: a survey of evidence, mechanisms and benefits. *Journal of Experimental Biology*, 204(14):2423–2430.

Laughlin, S. B., Howard, J., and Blakeslee, B. (1987). Synaptic limitations to contrast coding in the retina of the blowfly *Calliphora*. *Proceedings of the Royal Society of London. Series B, Biological Sciences*, 231(1265):437–467.

Marshall, J., Cronin, T. W., and Kleinlogel, S. (2007). Stomatopod eye structure and function: A review. *Arthropod Structure & Development*, 36(4):420–448.

Menzel, R. (1975). Polarisation sensitivity in insect eyes with fused rhabdoms. In Snyder, A. W. and Menzel, R., editors, *Photoreceptor Optics*, pages 372–387. Springer Berlin Heidelberg.

Moody, M. F. and Parriss, J. R. (1961). The discrimination of polarized light by Octopus: a behavioural and morphological study. *Zeitschrift für vergleichende Physiologie*, 44(3):268–291.

Nicol, D. and Meinertzhagen, I. A. (1982). An analysis of the number and composition of the synaptic populations formed by photoreceptors of the fly. *Journal of Comparative Neurology*, 207(1):29–44.

Nilsson, D.-E., Labhart, T., and Meyer, E. (1987). Photoreceptor design and optical properties affecting polarization sensitivity in ants and crickets. *Journal of Comparative Physiology*, 161(5):645–658.

Nilsson, D.-E., Land, M. F., and Howard, J. (1988). Optics of the butterfly eye. *Journal of Comparative Physiology*, 162(3):341–366.

Niven, J. E., Anderson, J. C., and Laughlin, S. B. (2007). Fly photoreceptors demonstrate energy-information trade-offs in neural coding. *PLoS Biology*, 5(4):e116.

Osorio, D. and Vorobyev, M. (1996). Colour vision as an adaptation to frugivory in primates. *Proceedings of the Royal Society of London. Series B, Biological Sciences*, 263(1370):593–599.

Pangršič, T., Stušek, P., Belušič, G., and Zupančič, G. (2005). Light dependence of oxygen consumption by blowfly eyes recorded with a magnetic diver balance. *Journal of Comparative Physiology A*, 191(1):75–84.

Shannon, C. (1948). A mathematical theory of communication. *Bell System Technical Journal*, 27(3):379–423.

Smola, U. and Meffert, P. (1979). The spectral sensitivity of the visual cells r7 and r8 in the eye of the blowfly *Calliphora erythrocephala*. *Journal of Comparative Physiology*, 133(1):41–52.

Smola, U. and Tscharntke, H. (1979). Twisted rhabdomeres in the dipteran eye. *Journal of Comparative Physiology*, 133(4):291–297.

Snyder, A. W. (1973). Polarization sensitivity of individual retinula cells. *Journal of Comparative Physiology*, 83(4):331–360.

Snyder, A. W. and Laughlin, S. B. (1975). Dichroism and absorption by photoreceptors. *Journal of Comparative Physiology*, 100(2):101–116.

Song, Z. and Juusola, M. (2014). Refractory sampling links efficiency and costs of sensory encoding to stimulus statistics. *The Journal of Neuroscience*, 34(21):7216–7237.

Song, Z., Postma, M., Billings, S. A., Coca, D., Hardie, R. C., and Juusola, M. (2012). Stochastic, adaptive sampling of information by microvilli in fly photoreceptors. *Current Biology*, 22(15):1371–1380.

Srinivasan, M. V., Laughlin, S. B., and Dubs, A. (1982). Predictive coding: A fresh view of inhibition in the retina. *Proceedings of the Royal Society of London B: Biological Sciences*, 216(1205):427–459.

Stavenga, D. G. (2004). Angular and spectral sensitivity of fly photoreceptors. III. dependence on the pupil mechanism in the blowfly *Calliphora*. *Journal of Comparative Physiology A*, 190(2):115–129.

Stavenga, D. G. (2010). On visual pigment templates and the spectral shape of invertebrate rhodopsins and metarhodopsins. *Journal of Comparative Physiology A*, 196(11):869–878.

Stavenga, D. G. and Arikawa, K. (2006). Evolution of color and vision of butterflies. *Arthropod Structure & Development*, 35(4):307–318.

Stavenga, D. G., Smits, R. P., and Hoenders, B. J. (1993). Simple exponential functions describing the absorbance bands of visual pigment spectra. *Vision Research*, 33(8):1011–1017.

Sterling, P. and Laughlin, S. B. (2015). *Principles of neural design*. MIT Press.

Stowe, S. (1983). A theoretical explanation of intensity-independent variation of polarisation sensitivity in crustacean retinula cells. *Journal of Comparative Physiology*, 153(4):435–441.

Strausfeld, N. J. and Wunderer, H. (1985). Optic lobe projections of marginal ommatidia in *Calliphora erythrocephala* specialized for detecting polarized light. *Cell Tissue Research*, 242(1):163–178.

Thomson, E. E. and Kristan, W. B. (2005). Quantifying stimulus discriminability: A comparison of information theory and ideal observer analysis. *Neural Computation*, 17(4):741–778.

van Steveninck, R. R. and Laughlin, S. B. (1996a). Light adaptation and reliability in blowfly photoreceptors. *International Journal of Neural Systems*, 7(4):437–444.

van Steveninck, R. R. and Laughlin, S. B. (1996b). The rate of information transfer at graded-potential synapses. *Nature*, 379(6566):642–645.

Vitzthum, H., Müller, M., and Homberg, U. (2002). Neurons of the central complex of the locust *Schistocerca gregaria* are sensitive to polarized light. *The Journal of Neuroscience*, 22(3):1114–1125.

Vorobyev, M. and Osorio, D. (1998). Receptor noise as a determinant of colour thresholds. *Proceedings of the Royal Society of London. Series B, Biological Sciences*, 265(1394):351–358.

Vorobyev, M., Osorio, D., Bennett, D. A. T., Marshall, J. N., and Cuthill, C. I. (1998). Tetrachromacy, oil droplets and bird plumage colours. *Journal of Comparative Physiology A*, 183(5):621–633.

Wada, S. (1974a). Spezielle randzonale Ommatidien der Fliegen (Diptera : Brachycera): Architektur und Verteilung in den Komplexauaen. *Zeitschrift für Morphologie der Tiere*, 77(2):87–125.

Wada, S. (1974b). Spezielle randzonale Ommatidien von *Calliphora erythrocephala meig.* (Diptera : Calliphoridae): Architektur der zentralen Rhabdomeren-kolumne und Topographie im Komplexauge. *International Journal of Insect Morphology and Embryology*, 3(3–4):397–424.

Warrant, E. J. and Nilsson, D.-E. (1998). Absorption of white light in photoreceptors. *Vision Research*, 38(2):195–207.

Wehner, R. (2001). Polarization vision – a uniform sensory capacity? *Journal of Experimental Biology*, 204(14):2589–2596.

Wunderer, H. and Smola, U. (1982a). Fine structure of ommatidia at the dorsal eye margin of *Calliphora erythrocephala meigen* (Diptera: Calliphoridae): An eye region specialised for the detection of polarized light. *International Journal of Insect Morphology and Embryology*, 11(1):25–38.

Wunderer, H. and Smola, U. (1982b). Morphological differentiation of the central visual cells R7/8 in various regions of the blowfly eye. *Tissue and Cell*, 14(2):341–358.

Wyszecki, G. and Stiles, W. S. (1982). *Color Science: Concepts and Methods, Quantitative Data and Formulae*. Wiley, 2nd edition.
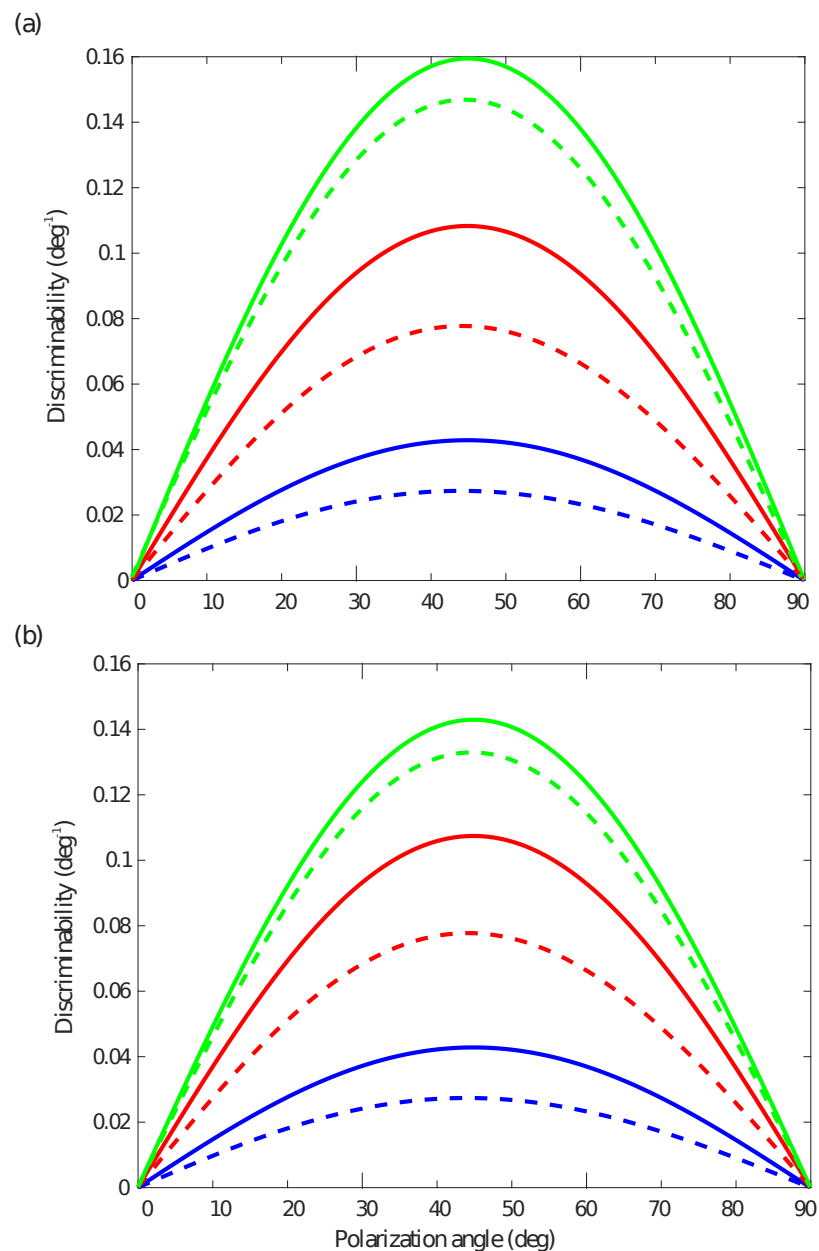
Figure 7. Discriminability as a function of polarization angle, θ, for light with degree of polarization $d = 0.1$, at three incident photon fluxes, N_i. a) Rhabdom length $L = 100\,\mu m$ with R7 and R8 of the same length, $\hat{l}_8 = 0.5$ (continuous lines) and with shorter R8, $\hat{l}_8 = 0.1$ (dashed lines). b) As (a), but taking into account tranduction unit saturation. Incident photon flux, N_i: 1×10^5 (blue), 3×10^5 (red), and 1×10^6 (green) photons s^{-1}.
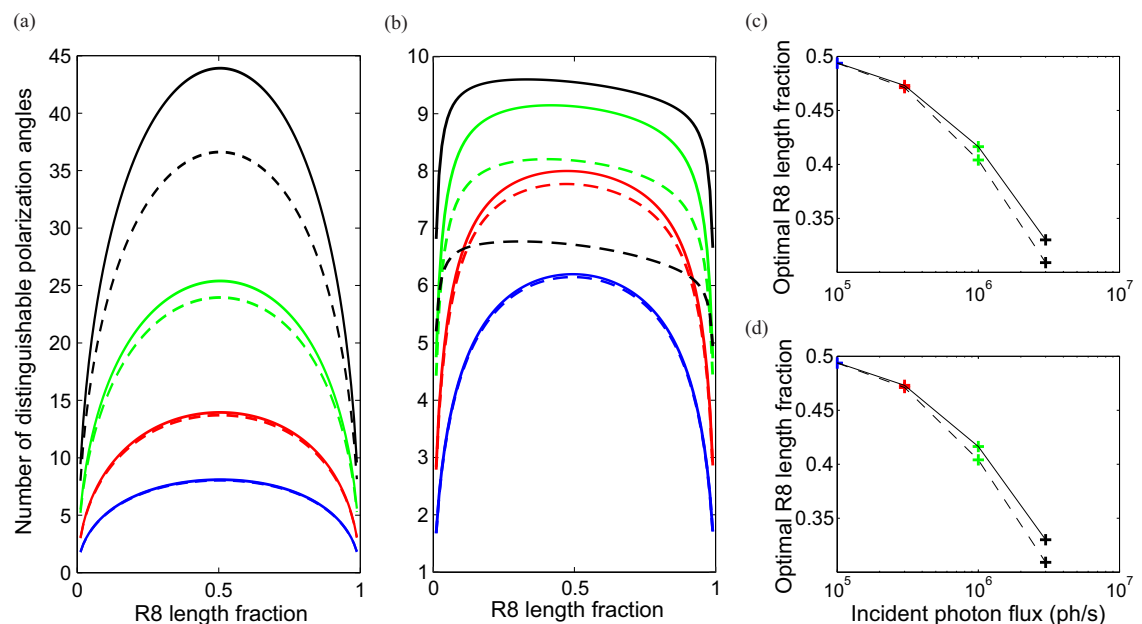
Figure 8. Optimum division of rhabdom between R7 and R8 maximizes two measures of coding ability, number of discriminable polarization angles and mutual information. Optima depend on light intensity (incident photon flux, N_i) and presence of intrinsic noise. (a) Discriminable polarization angles versus R8 length fraction in the absence of intrinsic noise without transduction unit saturation (solid curves) and with saturation (dashed curves). Four light intensities N_i; 1×10^5 (blue), 3×10^5 (red), 1×10^6 (green) and 3×10^6 (black) photons s^{-1}. (b) As in (a) but in the presence of intrinsic noise. Note the optimum division shifts to shorter R8 at higher intensities. (c) Optimum R8 length fractions from (b) versus incident photon flux without transduction unit saturation (solid curve) and with saturation (dashed curve). (d) As in (c), but R8 length optimizes mutual information.
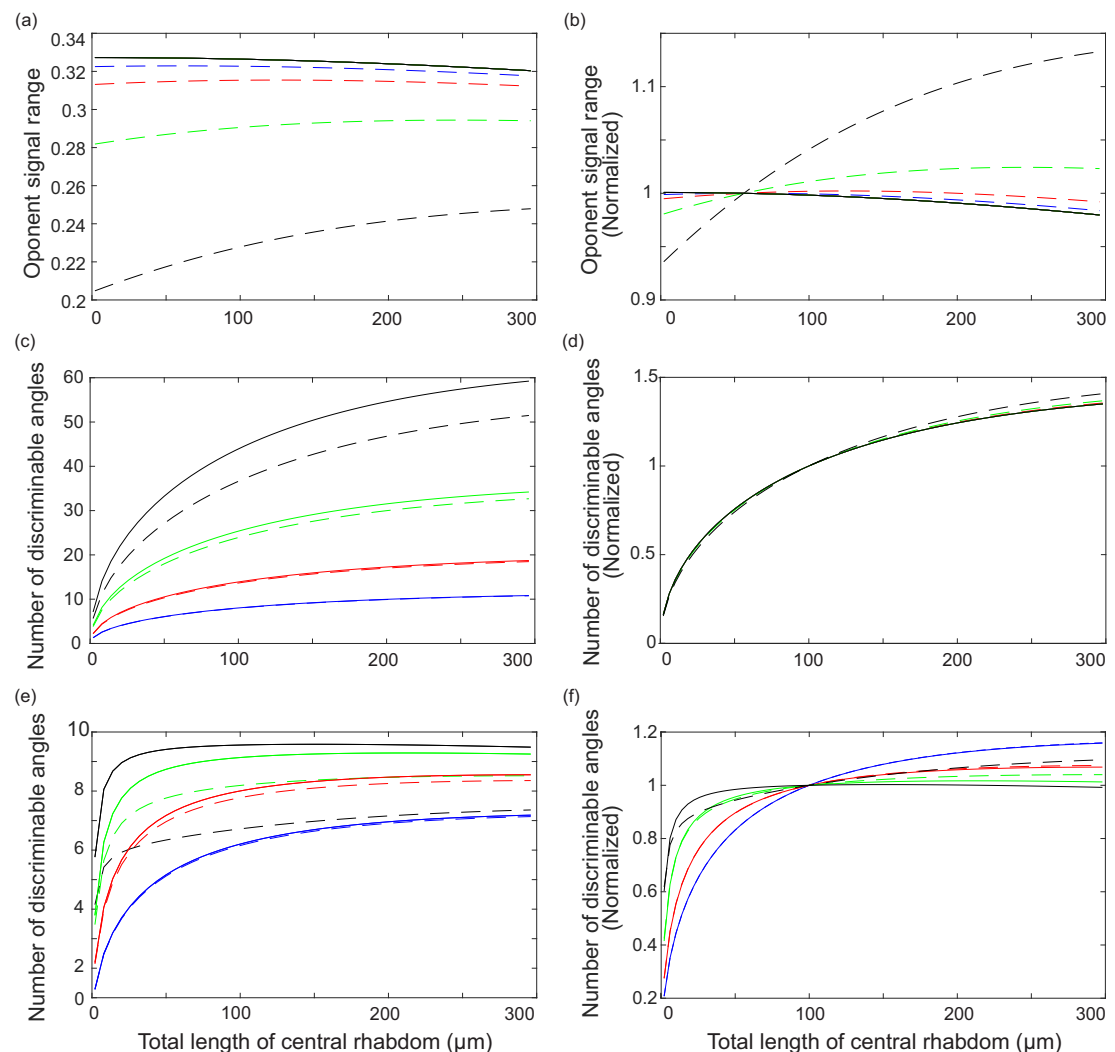
Figure 9. Ability of opponent unit to code polarization depends of rhabdom length, L, according to relationships that depend on light intensity, transduction unit saturation and the presence of intrinsic noise. Most relationships follow the Law of Diminishing Returns. (a) Opponent unit signal range (ΔQ) at four light intensities with transduction unit saturation (dashed) and without saturation (solid). Light intensities specified by incident photon flux, N_i photons s^{-1}; 1×10^5 (blue), 3×10^5 (red), 1×10^6 (green) and 3×10^6 (black). (b) Curves plotted in (a), each normalised to its value at $L = 100\,\mu$m. (c) Number of discriminable angles without intrinsic noise, N_i and saturation state as in (a) and (d) curves normalized to $L = 100\,\mu$m as in (b). (e) Number of discriminable angles as in (c), but with intrinsic noise σ_{in}. (f) Curves in (e) normalised to $L = 100$